NATIONAL ADVISORY COMMITTEE FOR AERONAUTICS

TECHNICAL NOTE

No. 1146

TESTS TO DETERMINE EFFECTS OF SLIPSTREAM ROTATION

ON THE LATERAL STABILITY CHARACTERISTICS OF A

SINGLE-ENGINE LOW-WING AIRPLANE MODEL

By Paul E. Purser and Margaret F. Spear

Langley Memorial Aeronautical Laboratory
Langley Field, Va.

NACA

Washington
September 1946

NATIONAL ADVISORY COMMITTEE FOR AERONAUTICS

TECHNICAL NOTE NO. 1146

TESTS TO DETERMINE EFFECTS OF SLIPSTREAM ROTATION

ON THE LATERAL STABILITY CHARACTERISTICS OF A

SINGLE-ENGINE LOW-WING AIRPLANE MODEL

By Paul E. Purser and Margaret F. Spear

SUMMARY

Tests have been made of a $\frac{1}{5}$-scale powered model of a single-engine low-wing airplane with three propeller-blade settings and three values of tail length to provide information on the effects of slipstream rotation on the directional stability and control characteristics of single-engine airplanes.

Estimates of lateral-force, rolling-moment, and yawing-moment coefficients due to slipstream rotation at zero pitch and yaw with flaps retracted were obtained from calculated slipstream characteristics and were found to compare favorably with test values except in cases for which the vertical tail is very near the effective edge of the displaced slipstream.

Analysis of the test results indicated that the slope of the yawing-moment curve at zero yaw decreased generally with the use of higher propeller blade angles (or torque coefficient), probably because the greater twist in the slipstream caused the vertical tail to stall at smaller positive angles of yaw and because of an increasing lateral displacement of the slipstream with increasing torque coefficient. The slope of the yawing-moment curve near zero yawing moment is probably a better indication of the directional stability under trim conditions. This slope increased with tail length and varied relatively little with changes in blade angle.

In general, the effective dihedral was the same for blade settings of 15° and 25° and smaller for the 35° setting.

The slope of the curve of lateral force against angle of yaw increased with blade angle and tail length for the model with tail off. With tail on, however, change of blade angle had a negligible effect on this parameter.

The angle of yaw at which rudder lock occurred did not vary
consistently with blade angle, torque coefficient, nor the value
of yawing-moment coefficient at zero yaw, and thus indicated a
necessity for using the full-scale thrust-torque relationship in
wind-tunnel tests made for determining the angle of yaw at which
rudder lock occurs.

Rudder-tab setting had a small effect on the angle of yaw at
which rudder lock occurred for the normal fuselage and the effect
was not consistent for the different values of blade setting.

INTRODUCTION

The NACA has undertaken a study of the problems of obtaining
adequate stability and control in climbing flight for high-
performance single-engine airplanes.

Among the stability and control problems existing in power-on
flight are those of obtaining adequate rudder and aileron control
for trim at low speeds and of preventing rudder lock (rudder-force
reversal). As a start toward the solution of these particular
problems a general series of wind-tunnel tests has been made of a
typical single-engine airplane model equipped with a single-rotating
propeller. Tests were made in the Langley 7- by 10-foot tunnel at
three values of tail length and three values of blade angle for a
thrust coefficient simulating the high-power climb condition. The
primary purpose of these tests was to provide data with which to
establish the validity of present methods for computing the out-of-
trim forces and moments produced by propeller operation through the
action of the slipstream on the vertical tail. A secondary purpose
was to determine the effects of not using the full-scale thrust-
torque relationship and rudder-trim-tab setting in wind-tunnel tests
made to determine the angle of yaw at which rudder lock will occur
on the airplane. The present paper reports these tests and the
analyses made for comparison with the test data.

COEFFICIENTS AND SYMBOLS

The results of the tests are presented as standard NACA coef-
ficients of forces and moments. Rolling-, yawing-, and pitching-
moment coefficients are given about the center-of-gravity location
shown in figure 1 (28.2 percent of the mean aerodynamic chord).
The data are referred to the stability axes, which are a system
of axes having its origin at the center of gravity and in which

the Z-axis is in the plane of symmetry and perpendicular to the relative wind; the X-axis is in the plane of symmetry and perpendicular to the Z-axis; and the Y-axis is perpendicular to the plane of symmetry. The positive directions of the stability axes, of angular displacements of the airplane and control surfaces, and of hinge moments are shown in figure 2.

The coefficients and symbols are defined as follows:

C_L lift coefficient $\left(\dfrac{\text{Lift}}{qS}\right)$

C_{L_V} lift coefficient of isolated vertical tail $\left(\dfrac{\text{Tail lift}}{qS_V}\right)$

C_X longitudinal-force coefficient $\left(\dfrac{X}{qS}\right)$

C_Y lateral-force coefficient $\left(\dfrac{Y}{qS}\right)$

C_l rolling-moment coefficient $\left(\dfrac{L}{qSb}\right)$

C_m pitching-moment coefficient $\left(\dfrac{M}{qSc'}\right)$

C_n yawing-moment coefficient $\left(\dfrac{N}{qSb}\right)$

c_l section lift coefficient $\left(\dfrac{l}{qc}\right)$

c_{d_0} section drag coefficient $\left(\dfrac{d_0}{qc}\right)$

T_c' effective thrust coefficient based on wing area $\left(\dfrac{T_{eff}}{qS}\right)$

C_T thrust coefficient $\left(\dfrac{T}{\rho n^2 D^4}\right)$

Q_c' torque coefficient based on wing area and span $\left(\dfrac{Q}{qSb}\right)$

C_Q torque coefficient $\left(\dfrac{Q}{\rho n^2 D^5}\right)$

V/nD propeller advance-diameter ratio

dC_T/dx differential thrust coefficient

dC_Q/dx differential torque coefficient

η propulsive efficiency $\left(\dfrac{T_{eff}V}{2\pi nQ}\right)$

H hinge moment, foot-pounds

Lift $= -Z$

$\left.\begin{array}{l}X\\Y\\Z\end{array}\right\}$ forces along axes, pounds (see fig. 2.)

$\left.\begin{array}{l}L\\M\\N\end{array}\right\}$ moments about axes, pound-feet (see fig. 2.)

l blade section lift, pounds

d_o blade section profile drag, pounds

T propeller thrust, pounds

T_{eff} propeller effective thrust, pounds

Q propeller torque, pound-feet

q free-stream dynamic pressure, pounds per square foot $\left(\rho V^2/2\right)$

q_t effective dynamic pressure at tail, pounds per square foot

q_s dynamic pressure behind the propeller, pounds per square foot

S wing area, square feet (9.40 on model)

S_v vertical-tail area, square feet (1.25 on model)

c airfoil section chord, feet

$\bar{c}$ average airfoil chord, feet

c' mean aerodynamic chord (M.A.C.), feet $\left(\dfrac{2}{S} \displaystyle\int_0^{b/2} c^2 \, db \right)$

b_v span of vertical tail, feet

b wing span, feet (7.509 on model)

$\dfrac{y}{b_v/2}$ spanwise station of vertical tail

L_a dimensionless quantity representing the additional lift at any point along the span of an airfoil

A aspect ratio

l_v tail length measured from center of gravity to quarter-chord point of vertical-tail mean aerodynamic chord

V air velocity, feet per second

D propeller diameter, feet (2.27 on model)

n propeller speed, revolutions per second

r radius to any propeller blade element

R propeller tip radius

x radial location of blade element (r/R)

x_t chordwise location of propeller-blade maximum thickness

ρ mass density of air, slugs per cubic foot

α angle of attack of thrust line, degrees

α_v angle of attack of vertical-tail chord, degrees

ψ angle of yaw, degrees

ψ_s angle of twist in propeller slipstream, degrees

i_t angle of stabilizer setting with respect to thrust line, degrees; positive when trailing edge is down

δ control-surface deflection, degrees

β propeller blade angle at 0.75 radius, degrees

θ propeller blade angle at radius r, degrees

Subscripts:

e   elevator

a   aileron

r   rudder

r_T rudder tab

v   vertical tail

t   values of force and moment coefficients provided by the tail

ψ partial derivative of a coefficient with respect to yaw
$$\left(\text{example:} \quad C_{l_\psi} = \frac{\partial C_l}{\partial \psi}\right)$$

α partial derivative of a coefficient with respect to angle of attack $\left(\text{example:} \quad C_{L_\alpha} = \frac{\partial C_L}{\partial \alpha}\right)$

MODEL AND APPARATUS

The model used was constructed with three interchangeable fuselage blocks in order to permit tests of three values of tail length (short, normal, and long). When arranged for the normal-tail configuration it is a $\frac{1}{5}$-scale model of a 37.5-foot-span single-engine low-wing airplane. The general physical characteristics of

the normal model are given in tables I and II. Three-view drawings
of the model and photographs showing the model mounted in the
Langley 7- by 10-foot tunnel (reference 1) are shown in figures 1
and 3, respectively.

The fuselage blocks for the short- and long-tail configura-
tions were developed by maintaining the same ordinates as for the
normal fuselage but the stations behind a point 30.1 inches behind
the propeller center line were contracted or expanded to provide
the required change in length.

Dimensions of the isolated vertical tail which was tested in
the Langley 4- by 6-foot vertical tunnel (reference 2) are given in
figure 4(a) and the test setup is shown in figure 4(b).

Power for the model was obtained from a 56-horsepower electric
motor, the speed of which was determined from an electric tachometer
which is accurate to within ±0.2 percent. The three-blade pro-
peller used was supplied with the model by the Bureau of Aeronautics,
Navy Department and appeared to be a $\frac{1}{5}$-scale model of an Aeroproducts
model no. A-20-156 reduced to 13.6-inch radius by removing 3 inches
from the tip and adding 1 inch at the root. Blade-form character-
istics measured from the model propeller are presented in figures 5
and 6.

TEST AND RESULTS

Test Conditions

The tests of the complete model were made in the Langley 7-
by 10-foot tunnel at a dynamic pressure of 4.09 pounds per square
foot, which corresponds to an airspeed of about 40 miles per hour.
The test Reynolds number was about 500,000 based on the wing mean
aerodynamic chord of 1.31 feet. Because of the turbulence factor
of 1.6 for the tunnel, the effective Reynolds number (for maximum
lift coefficients) was about 800,000.

The tests of the isolated vertical tail were made in the
Langley 4- by 6-foot vertical tunnel at a dynamic pressure of
15 pounds per square foot, which corresponds to an airspeed of about
76 miles per hour. The test Reynolds number was about 740,000 based
on the tail mean aerodynamic chord of 1.03 feet. Because of the
turbulence factor of 1.93 for the tunnel, the effective Reynolds
number (for maximum lift coefficients) was about 1,428,000.

Corrections

All the complete-model data have been corrected for tares caused by the model support strut. Jet-boundary corrections have been applied to the angles of attack, the longitudinal-force coefficients, and the tail-on pitching-moment coefficients. The corrections were computed as follows by use of reference 3:

$$\Delta\alpha = 1.065 C_L$$

$$\Delta C_X = -0.0157 C_L^2$$

For the short tail

$$\Delta C_m = -7.74 C_L\left(\frac{0.184}{\sqrt{q_t/q}} - 1.16\right)\left(\frac{\partial C_m}{\partial i_t}\right)$$

For the normal tail

$$\Delta C_m = -7.74 C_L\left(\frac{0.206}{\sqrt{q_t/q}} - 1.16\right)\left(\frac{\partial C_m}{\partial i_t}\right)$$

For the long tail

$$\Delta C_m = -7.74 C_L\left(\frac{0.222}{\sqrt{q_t/q}} - 1.16\right)\left(\frac{\partial C_m}{\partial i_t}\right)$$

where $\Delta\alpha$ is in degrees. All jet-boundary corrections were added to the test data.

The lift coefficients of the isolated vertical tail have been corrected for tares caused by the model support strut. Jet-boundary corrections derived in a manner similar to that used in reference 4 have been applied to the angles of attack as follows:

$$\Delta\alpha_V = 0.71 C_{L_V}$$

where $\Delta\alpha$ is in degrees and was added to the test angle of attack.

Test Procedure

Propeller calibrations were made by measuring the longitudinal force of the model with flaps and landing gear retracted and tail

off at an angle of attack of 0° for a range of propeller speed for
values of propeller blade setting β of 15°, 25°, and 35°. Thrust
coefficients were determined from the relation

$$T_c{}' = C_{X_{propeller\ operating}} - C_{X_{propeller\ removed}}$$

The torque coefficients were computed by use of a calibration of
motor torque as a function of minimum current. The results of the
model propeller calibrations are presented in figure 7.

Power-on yaw tests were made at approximately 0° angle of
attack and with flaps retracted for each propeller blade setting at
a value of $T_c{}'$ of about 1.25, which corresponds to about 1500 horse-
power for a 37.5-foot-span full-scale airplane at a lift coefficient
of 2.5 for a wing loading of 31.25 pounds per square foot. Figure 8
presents a plot of the horsepower represented for various wing loadings
and model scales. The tests were made with the rudder fixed at zero,
rudder free with tab set at 0° and 20°, and tail off.

Presentation of Results

An outline of the figures presenting the results of the tests
and analyses follows:

COMPUTATION PROCEDURES

Slipstream

In order to aid in the analysis of the test results, the distributions of thrust, torque, and slipstream rotation along the propeller blade were computed by means of methods outlined in references 5 to 7. The lift and drag characteristics of the propeller blade sections were estimated from the measured values of thickness h/b, position of maximum thickness x_t, trailing-edge angle ϕ, maximum camber m, and position of maximum camber p (figs. 5 and 6) by use of the data in references 8 to 10. The blade section lift and drag characteristics are presented in figure 9 and the computed values of thrust and torque distributions along the propeller blade are presented in figure 10(a). The computed thrust distributions were adjusted by the ratio of the measured values of C_T to the computed values of C_T and the computed torque distributions were adjusted by the ratio of the measured values of C_Q to the computed values of C_Q. Adjusted values are presented in figure 10(b). Dynamic-pressure ratios and slipstream-rotation distributions computed from the adjusted values of dC_T/dx and dC_Q/dx are presented in figure 11. These results represent distribution values immediately behind the propeller.

Vertical-Tail Lift

It has been estimated (reference 11) that a wing behind the propeller may diminish the angle of twist in the slipstream by 50 percent. Hence the angle-of-attack distribution for the vertical tail was assumed to be one-half the distribution of slipstream twist behind the propeller $\left(\text{that is, } \alpha_V = \frac{1}{2}\psi_s\right)$.

For a first approximation, a curve was drawn having ordinates at each spanwise station $\dfrac{y}{b_V/2}$, of

$$\frac{cq_s}{cq}\, \alpha_V\, cl_{\alpha_V} \tag{1}$$

where $c_{l_{\alpha_V}}$ is the section lift-curve slope. Since downwash tends to make the lift distribution assume an elliptical shape (reference 12), the ordinates of this curve were averaged with the ordinates of a semiellipse having the same total area under the curve. In order to obtain a curve having ordinates representing some known quantity, the ordinates of the average curve were reduced so that the area under the curve was 2. The ordinates of the resulting curve were then designated L_a (reference 13), which corresponds to $\dfrac{cc_l A}{bC_L}$, because it can be shown that

$$\int_{-1.0}^{1.0} L_a \; d\frac{y}{b_V/2} = 2.0 \tag{2}$$

The values of L_a were then used in a second approximation to the lift coefficient according to the relation

$$C_{L_V} = \frac{C_{L_{\alpha_V}}}{2} \int_{-1.0}^{1.0} L_a \alpha_V \frac{q_s}{q} \; d\frac{y}{b_V/2} \tag{3}$$

where $C_{L_{\alpha_V}}$ is the lift-curve slope of the isolated vertical tail measured from figure 12. The data for the isolated vertical tail were used because tests showed that for this configuration the addition of the horizontal tail did not increase the lift-curve slope of the vertical tail. This result is probably due to the cancelation by mutual interference of any small effect that might be expected from the relatively high location and narrow chord of the horizontal tail.

Curves obtained from equation (3) were integrated to obtain the values of tail lift coefficient.

In order to make some allowance for change in dynamic-pressure ratio between the region directly behind the propeller and the region around the vertical tail, the propeller-slipstream flow was considered comparable to flow in an axially symmetrical heated jet of air. On figures 9 to 12 of reference 14, a line was drawn to represent the span of the vertical tail as 17.8 percent greater than the radius of the jet. (The span of the vertical tail is 17.8 percent greater than the radius of the model propeller.) Each

velocity-ratio area within this line and outside this line was
measured. The square of the ratio of the total area to the area
within the line was computed and plotted against longitudinal
traverse. The resulting values of this ratio were 1.07, 1.12,
and 1.20 for the short, normal, and long tails, respectively.
Each vertical-tail lift coefficient was divided by these values to
obtain the final values of C_{L_V}. No attempt was made to account for
changes in the twist or twist distribution caused by spreading of
the slipstream.

<center>Forces and Moments Contributed by the</center>

<center>Vertical Tail and the Slipstream</center>

Lateral force.- Lateral-force coefficients due to lift on the
vertical tail in the slipstream at zero yaw C_{Y_t} were computed
for the three test blade angles and three tail lengths as

$$C_{Y_t} = \frac{C_{L_V} S_V}{S}$$

Yawing moment.- Yawing-moment coefficients produced by lift
on the vertical tail in the slipstream at zero yaw C_{n_t} were
computed for the various blade angles and tail lengths as

$$C_{n_t} = - \frac{C_{L_V} S_V l_V}{Sb}$$

Rolling moment.- The tail-off rolling-moment coefficient at
zero yaw $\left(C_{l_{\psi=0}}\right)_{\text{tail off}}$ was computed as $-\frac{1}{2}Q_c'$ on the assumption
that the wing absorbed 50 percent of the slipstream rotation. (See
reference 11.) The increment of rolling-moment coefficient due to
lift on the vertical tail was obtained by graphical integration of
the computed vertical-tail lift distribution (moments measured
about line through center of gravity, parallel to thrust line).
This increment was added to the computed tail-off value for the
tail-on rolling-moment coefficient.

No satisfactory method was found for estimating tail-off
values of lateral-force and yawing-moment coefficients at zero yaw.

The out-of-trim values of C_Y are relatively unimportant, however, since they correspond to rather small angles of bank. The out-of-trim tail-off values of C_n, although small for the model as tested, can be fairly large when the flaps are deflected. Consequently, for the flap-down conditions, the yawing moments induced by the slipstream acting on the flaps should be considered.

DISCUSSION

Comparison of Computed and Measured Coefficients

Force and moment coefficients measured at zero yaw were taken from test data presented in figures 14 to 16.

Computed values of lateral-force coefficient are presented in figure 13 and compared with the test values. The test values generally agreed with the computed values within 10 to 15 percent except for the case of the long tail with $\beta = 35°$. The disagreement is probably a result of the nearness of the tail to the edge of the slipstream which was laterally displaced by the action of the wing in shearing the rotating stream. This displacement was necessarily neglected in the computations.

Computed values of yawing-moment coefficient produced by vertical-tail lift C_{n_t} are presented in figure 13 and compared with values of $\left(C_{n_t}\right)_{\psi=0}$ measured from test data. The greatest disagreement occurred at $\beta = 35°$ for the long fuselage, the test value being about 30 percent smaller than the computed value. This difference also is probably caused by the lateral displacement of the slipstream.

Rolling-moment coefficients from computations and from test results are compared in figure 13. Since test values of $\left(C_{l_{\psi=0}}\right)_{\text{tail off}}$ vary from 50 to 60 percent of the torque coefficient $Q_c{}'$, the amount of slipstream twist absorbed by the wing-fuselage combination was overestimated in the computations; thus, test values for tail-off rolling-moment coefficient were more negative than estimated values. Slightly better agreement might have been obtained had some attempt been made to compute the span loading induced by the slipstream instead of using the simpler relation of $\frac{1}{2}Q_c{}'$. The increment of rolling moment due to the tail was underestimated; therefore, test values of tail-on rolling-moment

coefficients were less negative than computed values. One reason
for the difference may be the effect of the horizontal tail in
producing a positive rolling moment; this effect was neglected in
computations.

For most models at zero pitch and yaw a typical value
of $\partial C_l/\partial \delta_a$ would be about 0.002. About 16° total aileron deflec-
tion would thus be required to trim out the rolling moment on the
complete model with the propeller operating at $\beta = 35°$. In cases
for which the aileron power appears to be marginal it would be wise
to make more accurate estimations of the rolling moment.

It may be concluded, from the foregoing discussion, that
reasonably accurate estimates of lateral force and rolling and
yawing moments induced by the slipstream at zero pitch and yaw
with flaps retracted may be made by using existing methods of
analysis except in cases for which the slipstream is displaced
laterally far enough to cause its effective edge to be very near the
vertical tail.

Stability

Directional stability.- Values of $C_{n\psi}$ at $C_n = 0$ and at $\psi = 0$,
measured from figures 14(b), 15(b), and 16(b), are presented in the
following table:

Tail length	$\beta = 15°$		$\beta = 25°$		$\beta = 35°$	
	$\psi = 0$	$C_n = 0$	$\psi = 0$	$C_n = 0$	$\psi = 0$	$C_n = 0$
Short	-0.0013	-0.0025	-0.0013	-0.0025	-0.0008	-0.0028
Normal	-.0028	-.0044	-.0023	-.0049	-.0010	-.0043
Long	-.0035	-.0100	-.0014	-.0087	-.0003	-.0084

As may be seen, directional stability at $\psi = 0$ decreased in
general with higher blade angle. Since, for a given tail length,
the values of $C_{n\psi}$ at $C_n = 0$ are almost equal, this decrease in
stability appears to be due to the vertical-tail stall occurring at
smaller yaw angles in the positive yaw range because of greater
twist of the slipstream. Examination of the curves indicates that
increasing tail length placed the tail nearer the edge of the
displaced slipstream so that the vertical tail effectively passed
out of the slipstream between 0° and 5° yaw on the long fuselage
with $\beta > 15°$.

The value of C_{n_ψ} at $C_n = 0$ is probably a better indication of the directional stability under trim conditions than is the value of C_{n_ψ} at $\psi = 0$. Values of C_{n_ψ} at $C_n = 0$ increased with tail length and were relatively unaffected by changes in blade angle.

Effective dihedral.- The slopes of the rolling-moment curves between -5° and 5° yaw were measured on figures 14(b), 15(b), and 16(b) to determine how effective dihedral varied with blade angle. For the short fuselage the rolling-moment curves were very nearly parallel. For the normal and long tails the slopes of the rolling-moment curves, however, remained constant for blade angles of 15° and 25° and decreased for the blade angle of 35°. The decrease amounted to not more than $2\frac{1}{2}°$ effective dihedral, based on the assumption that a value of C_{l_ψ} of 0.0002 is equivalent to 1° effective dihedral. This decrease for the long tail indicates that the tail was near the edge of the displaced slipstream, which agrees with the conclusion reached from the yawing-moment curves.

Lateral force.- The tests showed that the lateral-force parameter C_{Y_ψ} near zero yaw for the tail-off curves (figs. 14(a) 15(a), and 16(a)) increased with blade angle and tail length, as would normally be expected. Changing the blade angle had a negligible effect on C_{Y_ψ} for the tail-on tests. Apparently the increase in the side-force variation with yaw produced by propeller operation at higher blade angles was canceled by a greater rate of change of sidewash with yaw at higher blade angles.

Rudder-free characteristics.- From the data of figures 14(c), 15(c), and 16(c) the value of C_n at zero yaw can be seen to increase nonlinearly with blade angle or torque coefficient. No consistent variation is apparent between angle of yaw at which rudder lock occurred and blade angle, torque coefficient, or yawing moment at zero yaw. This inconsistency indicates that, in order to predict rudder lock for a full-scale airplane from wind-tunnel data, tests of the wind-tunnel model should be made under conditions corresponding to the thrust-torque relationship of the full-scale airplane. An attempt should also be made to reproduce the full-scale thrust-coefficient and torque-coefficient distribution along the blade although, in general, small changes in the distribution should have only secondary effects on the results.

Effect of rudder tab.- Comparison of the yawing-moment curves of rudder-free tests for two rudder-tab settings on the model with normal fuselage (figs. 15(c) and 15(d)) shows that a large positive

tab setting was insufficient for trim and that it had a relatively
small and inconsistent effect in increasing the negative angle of
yaw at which rudder lock occurred. A large tab would have more
effect on trim and might have more effect on the angle of yaw at
which rudder lock occurred.

CONCLUSIONS

The results of wind-tunnel tests of a single-engine low-wing
airplane model equipped with a single-rotating propeller indicated
the following conclusions:

1. Values, at zero pitch and yaw with flaps retracted, of
lateral-force and yawing-moment coefficients contributed by the
tail and of rolling-moment coefficients may be estimated with
reasonable accuracy from calculations of slipstream characteristics
except in cases in which the vertical tail is very near the edge of
the displaced slipstream.

2. The slope of the yawing-moment curve near zero yaw decreased
as the propeller blade angle increased probably because of the
lateral displacement of the slipstream. The slope of the yawing-
moment curve near zero yawing moment (probably a better indication
of directional stability) increased with increasing tail length
and was relatively unaffected by changes in blade angle.

3. In general, the effective dihedral was the same for blade
angles of 15° and 25° and decreased for a blade setting of 35°.

4. Tail-off tests showed an increase in the slope of the
lateral-force curve with increased blade angle and tail length.

5. Yawing-moment curves of rudder-free tests indicated the
necessity of using full-scale thrust-torque relationships on models
used in wind-tunnel tests for determining the angle of yaw at which
rudder lock will occur.

6. Rudder-tab setting had a small effect on the angle of yaw
at which rudder lock occurred for the normal fuselage and the
effect was not consistent for the different values of blade setting.

Langley Memorial Aeronautical Laboratory
        National Advisory Committee for Aeronautics
            Langley Field, Va., July 16, 1946

REFERENCES

1. Wenzinger, Carl J., and Harris, Thomas A.: Wind-Tunnel Investigation of an N.A.C.A. 23012 Airfoil with Various Arrangements of Slotted Flaps. NACA Rep. No. 664, 1939.

2. Ames, Milton B., Jr., and Sears, Richard I.: Pressure-Distribution Investigation of an N.A.C.A. 0009 Airfoil with a 30-Percent-Chord Plain Flap and Three Tabs. NACA TN No. 759, 1940.

3. Gillis, Clarence L., Polhamus, Edward C., and Gray, Joseph L., Jr.: Charts for Determining Jet-Boundary Corrections for Complete Models in 7- by 10-Foot Closed Rectangular Wind Tunnels. NACA ARR No. L5G31, 1945.

4. Swanson, Robert S., and Schuldenfrei, Marvin J.: Jet-Boundary Corrections to the Downwash behind Powered Models in Rectangular Wind Tunnels with Numerical Values for 7- by 10-Foot Closed Wind Tunnels. NACA ARR, Aug. 1942.

5. Stickle, George W., and Crigler, John L.: Propeller Analysis from Experimental Data. NACA Rep. No. 712, 1941.

6. Crigler, John L.: Comparison of Calculated and Experimental Propeller Characteristics for Four-, Six-, and Eight-Blade Single-Rotating Propellers. NACA ACR No. 4B04, 1944.

7. Crigler, John L., and Talkin, Herbert W.: Charts for Determining Propeller Efficiency. NACA ACR No. L4I29, 1944.

8. Jacobs, Eastman N., Ward, Kenneth E., and Pinkerton, Robert M.: The Characteristics of 78 Related Airfoil Sections from Tests in the Variable-Density Wind Tunnel. NACA Rep. No. 460, 1933.

9. Jacobs, Eastman N., and Sherman, Albert: Airfoil Section Characteristics as Affected by Variations of the Reynolds Number. NACA Rep. No. 586, 1937.

10. Pinkerton, Robert M., and Greenberg, Harry: Aerodynamic Characteristics of a Large Number of Airfoils Tested in the Variable-Density Wind Tunnel. NACA Rep. No. 628, 1938.

11. Biermann, David, and Hartman, Edwin P.: Wind-Tunnel Tests of Four- and Six-Blade Single- and Dual-Rotating Tractor Propellers. NACA Rep. No. 747, 1942.

12. Schrenk, O.: A Simple Approximation Method for Obtaining the
      Spanwise Lift Distribution. NACA TM No. 948, 1940.

13. Anderson, Raymond F.: Determination of the Characteristics of
      Tapered Wings. NACA Rep. No. 572, 1936.

14. Corrsin, Stanley: Investigation of Flow in an Axially Symmetrical
      Heated Jet of Air. NACA ACR No. 3L23, 1943.

TABLE I

MODEL WING AND TAIL-SURFACE DATA

	Wing	Horizontal tail	Vertical tail
Area, sq ft	9.40	2.15	[a]1.25
Span, ft	7.509	3.33	1.335
Aspect ratio	6.00	5.16	1.30
Taper ratio	2.00	----------	----------
Dihedral of chord plane, deg:			
Inboard panel	-0.73	0	----------
Outboard panel	7.75	0	----------
Sweepback, quarter-chord line, deg	0	----------	----------
Root section	NACA 66,2-216	NACA 64,2-015 (modified)	NACA 64,2-015 (modified)
Break section	NACA 66,2-216	----------	----------
Tip section	NACA 66,2-216	NACA 64,2-012 (modified)	NACA 64,2-012 (modified)
[b]Angle of incidence at root, deg . .	0	----------	----------
[b]Angle of incidence at break, deg . .	0	----------	----------
[b]Angle of incidence at tip, deg . . .	0	----------	----------
Mean aerodynamic chord, ft	1.31	0.68	1.03
Root chord, ft	1.68	0.84	1.35
Theoretical tip chord, ft	0.34	0.47	0.59

[a]Includes no dorsal-fin area.

[b]Angle of incidence measured with respect to thrust line.

NATIONAL ADVISORY
COMMITTEE FOR AERONAUTICS

TABLE II

MODEL CONTROL-SURFACE DATA

	Elevators	Rudder
Area, behind hinge line, sq ft	0.592	0.371
Balance area, sq ft . . . , ...	0.158	0.102
Root-mean-square chord, behind hinge line, ft	0.198	0.32
Distance to hinge line from normal c.g., ft	3.56	3.68
Control deflection, deg	30 up, 20 down	30 right, 30 left
Trim-tab area, sq ft	0.0012	0.00053
Tab deflection, deg	±15	±23

NATIONAL ADVISORY
COMMITTEE FOR AERONAUTICS
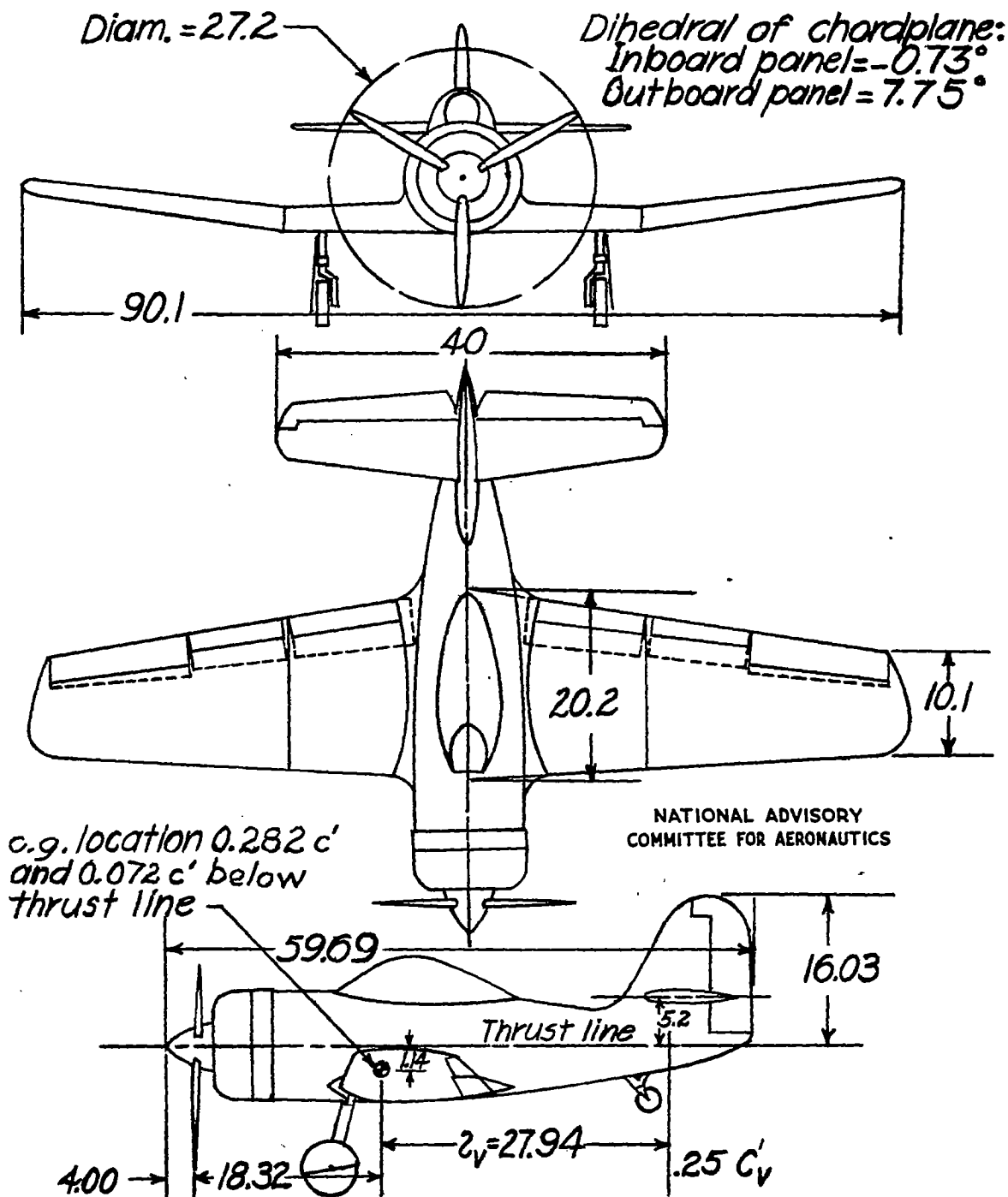
(a) Short tail.

Figure 1.- Drawings of the single-engine airplane model
   showing the three tail lengths. (All dimensions are in
   inches.)

71.02

Thrust line

$l_v = 39.27$

$.25\ C'_v$
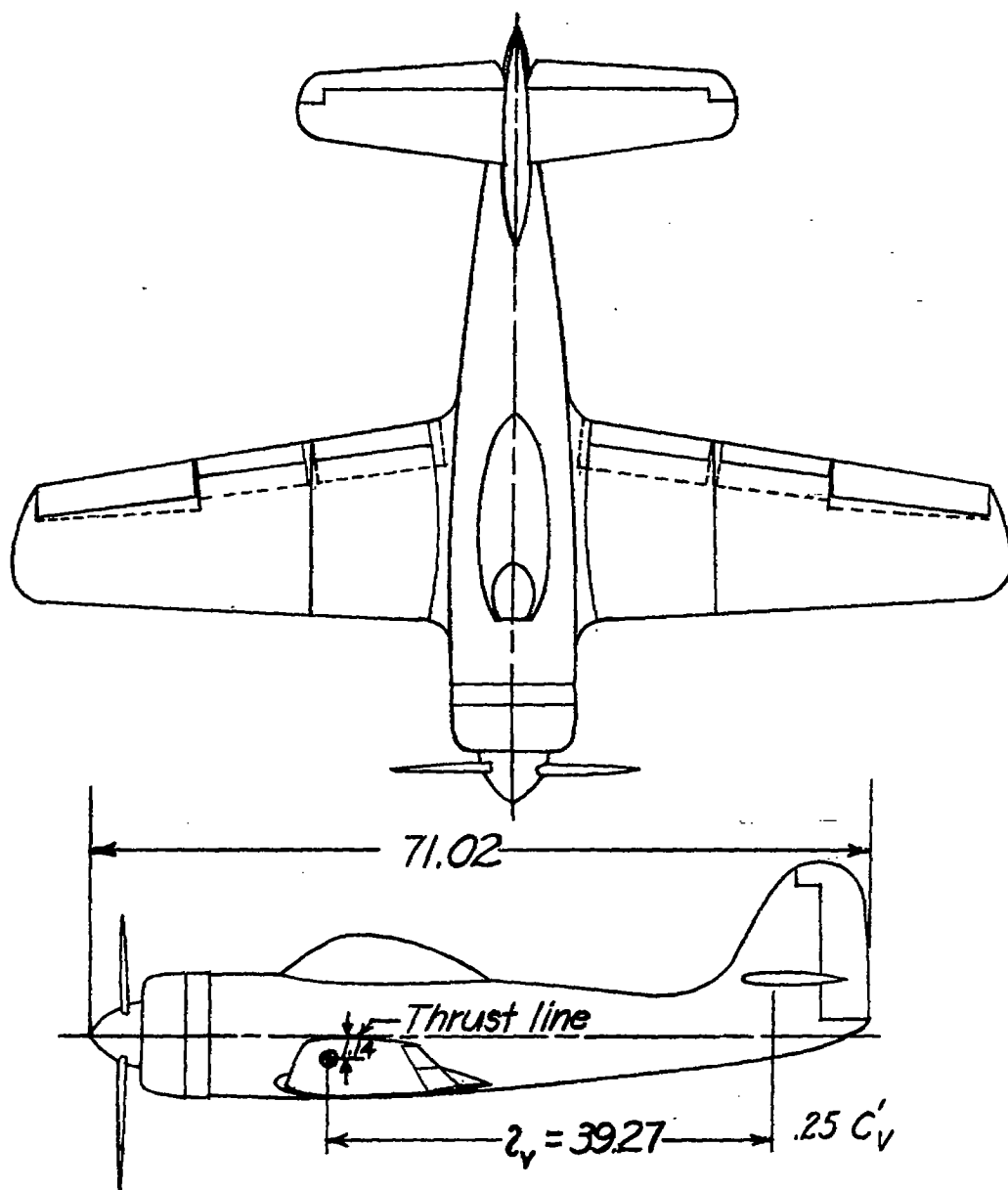
NATIONAL ADVISORY
COMMITTEE FOR AERONAUTICS

(b) Normal tail.

Figure 1.- Continued.

NATIONAL ADVISORY
COMMITTEE FOR AERONAUTICS

91.13

Thrust line

$l_v = 59.38$

.25 C_v'
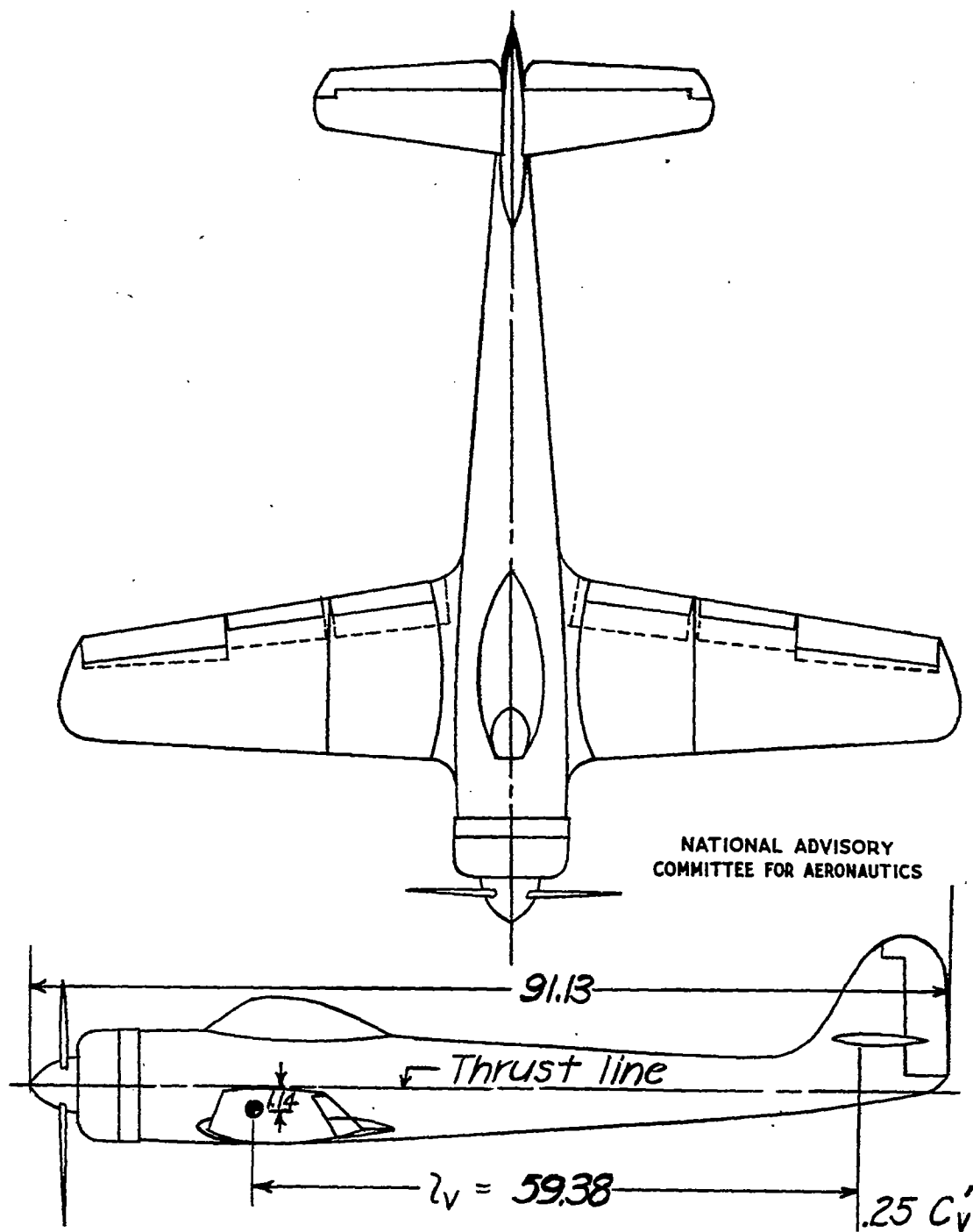
(c) Long tail.

Figure 1.- Concluded.

Fig. 2   NACA TN No. 1146
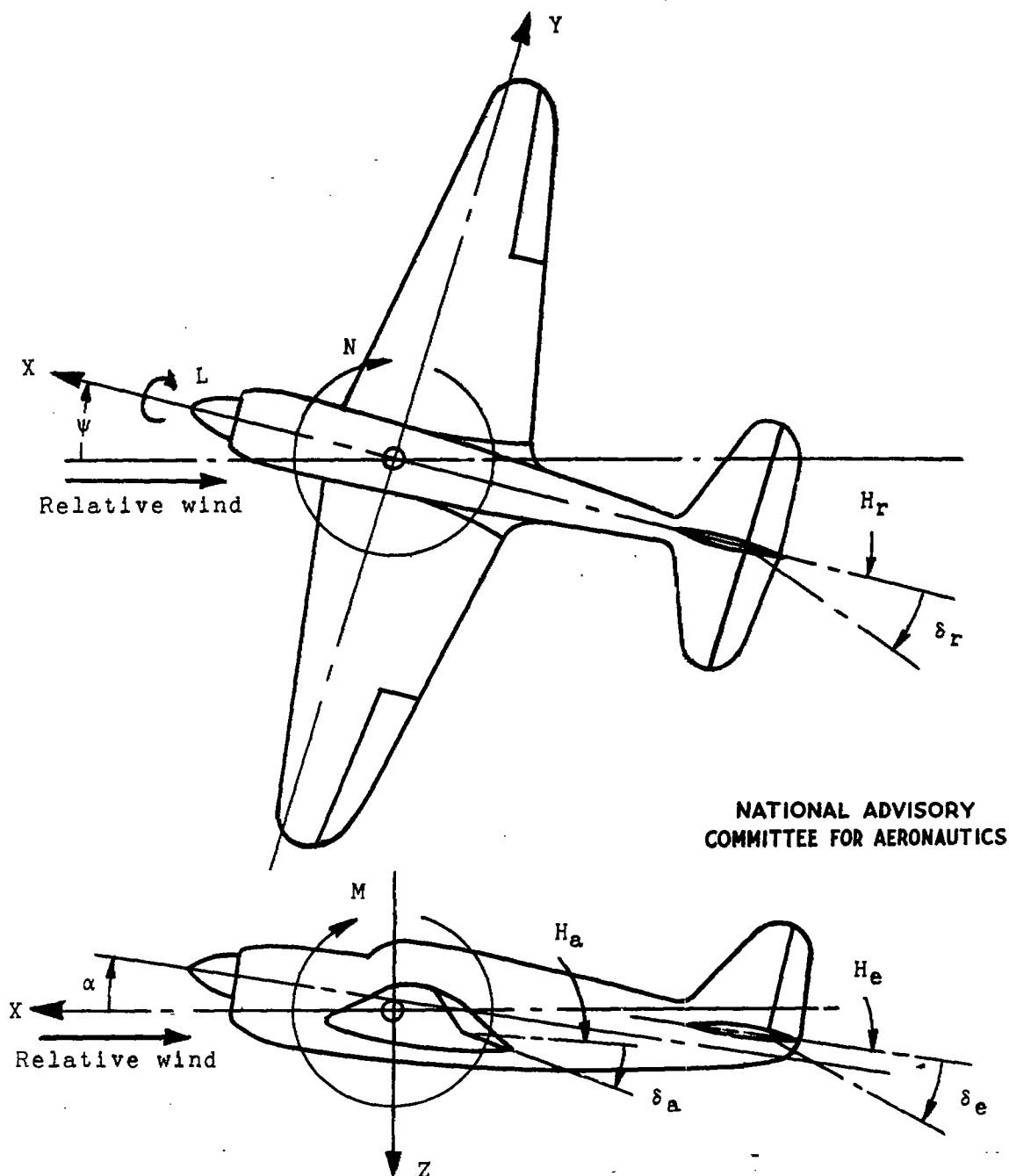
Figure 2 .- System of axes and control-surface hinge moments and deflections. Positive values of forces, moments, and angles are indicated by arrows. Positive values of tab hinge moments and deflections are in the same directions as the positive values for the control surfaces to which the tabs are attached.

(a) Short tail. $\dfrac{l_v}{b} = 0.310$

(b) Normal tail. $\dfrac{l_v}{b} = 0.436$

(c) Long tail. $\dfrac{l_v}{b} = 0.659$

Figure 3.- Photographs of the single-engine airplane model showing the three tail lengths tested.
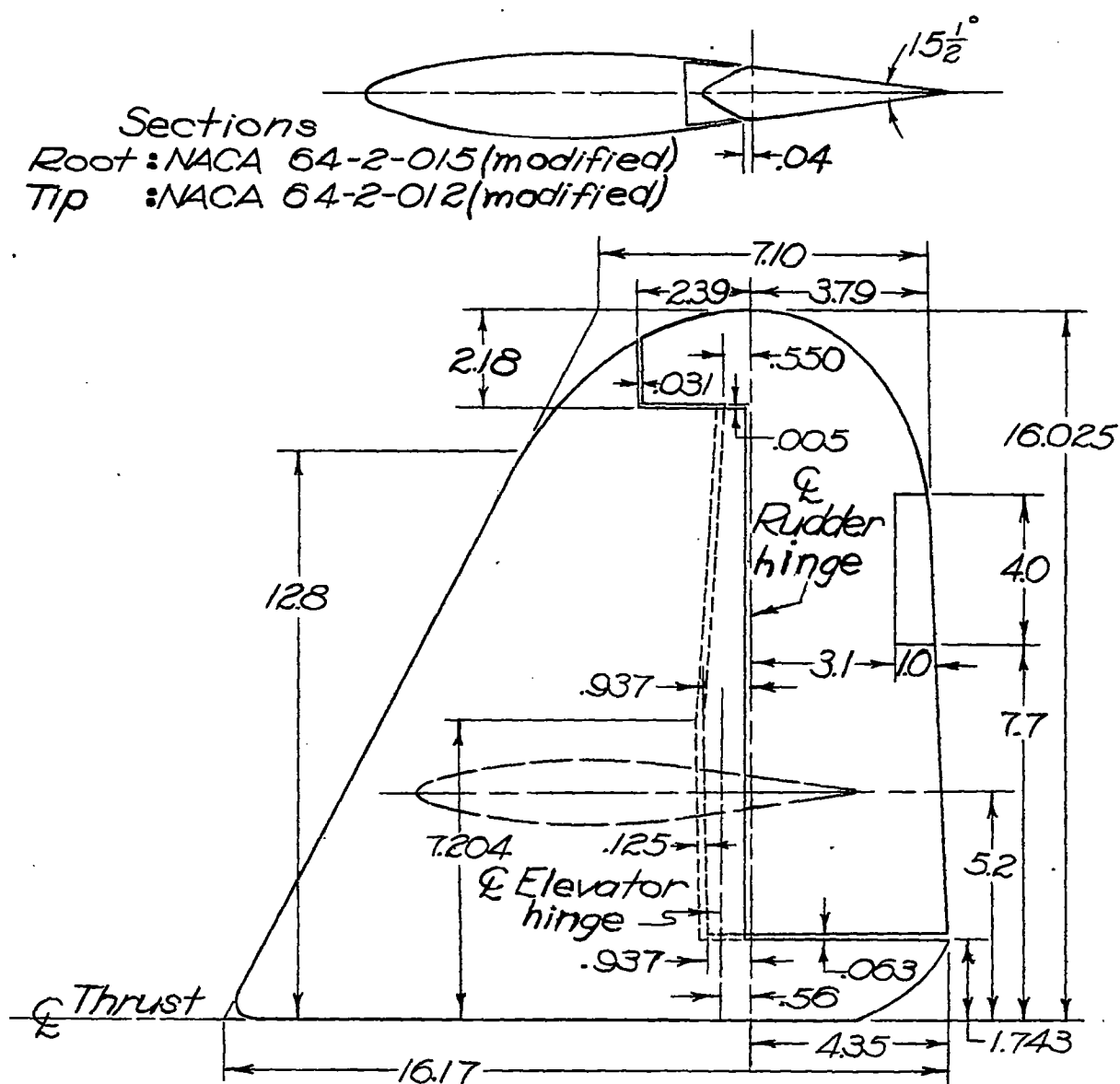
(a) Model.

Figure 4.- Isolated vertical tail of the single-engine
low-wing fighter model.(All dimensions are in inches.)

Wind
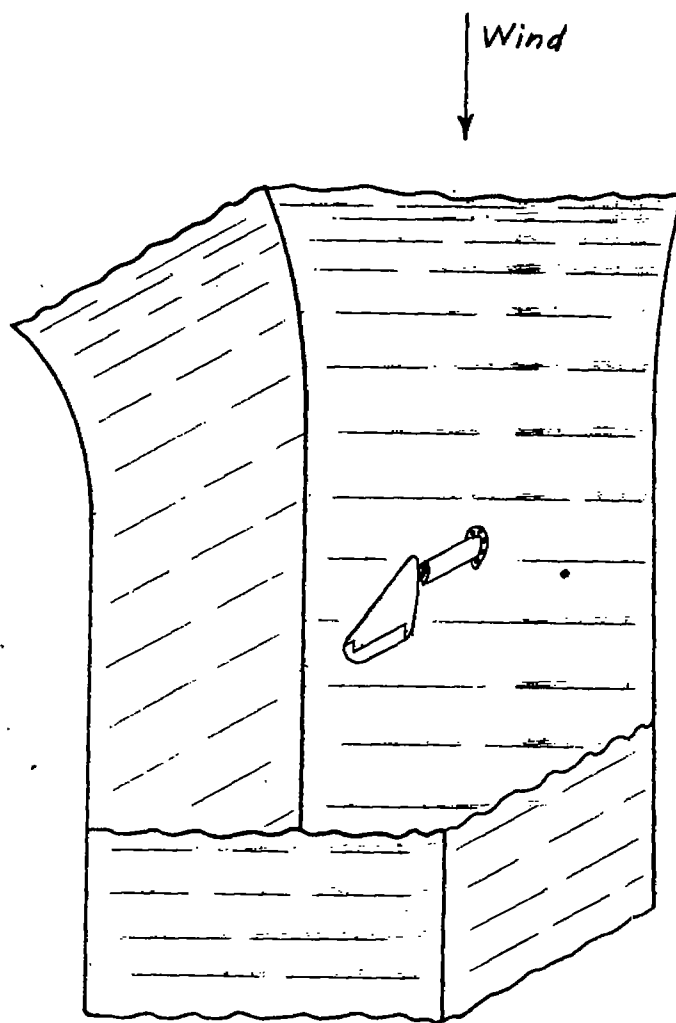
NATIONAL ADVISORY
COMMITTEE FOR AERONAUTICS.

(b) Test setup.

Figure 4.- Concluded.
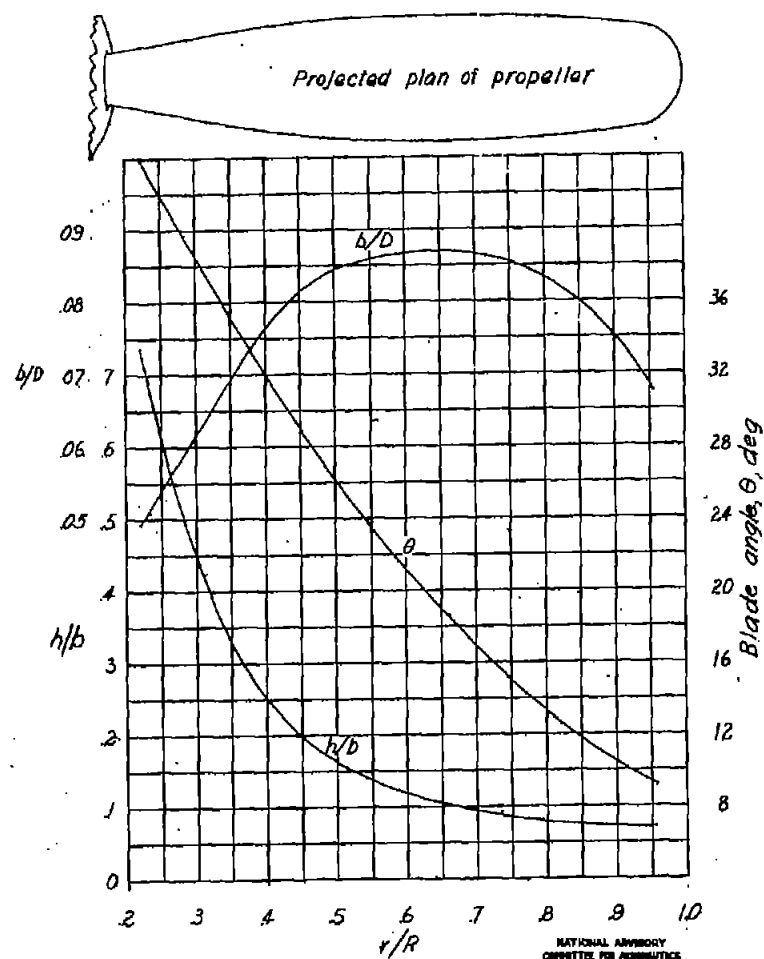
Figure 5.- Plan-form and blade-form curves for the propeller used on the single-engine low-wing fighter model. D, diameter; R, radius; r, station radius; b, section chord; h, section thickness; θ, blade angle.
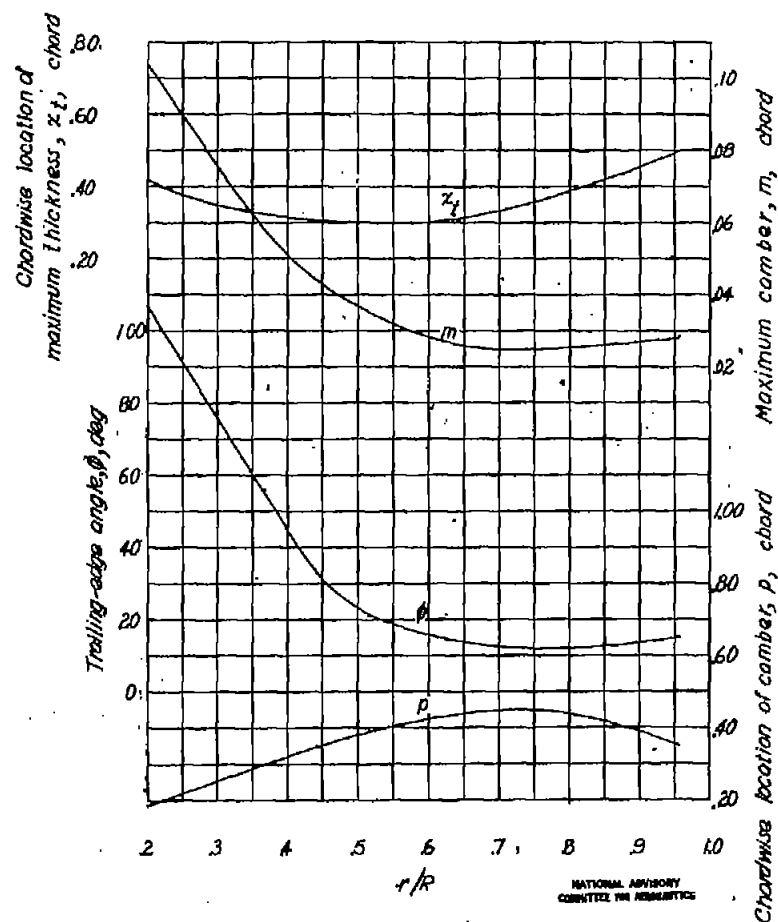
Figure 6.- Curves of chordwise location of maximum thickness z_t, maximum camber m, chordwise location of maximum camber p, and trailing-edge angle θ against radial location of blade element r/R for the propeller used on the single-engine low-wing fighter model; R, blade radius; r, section radius.
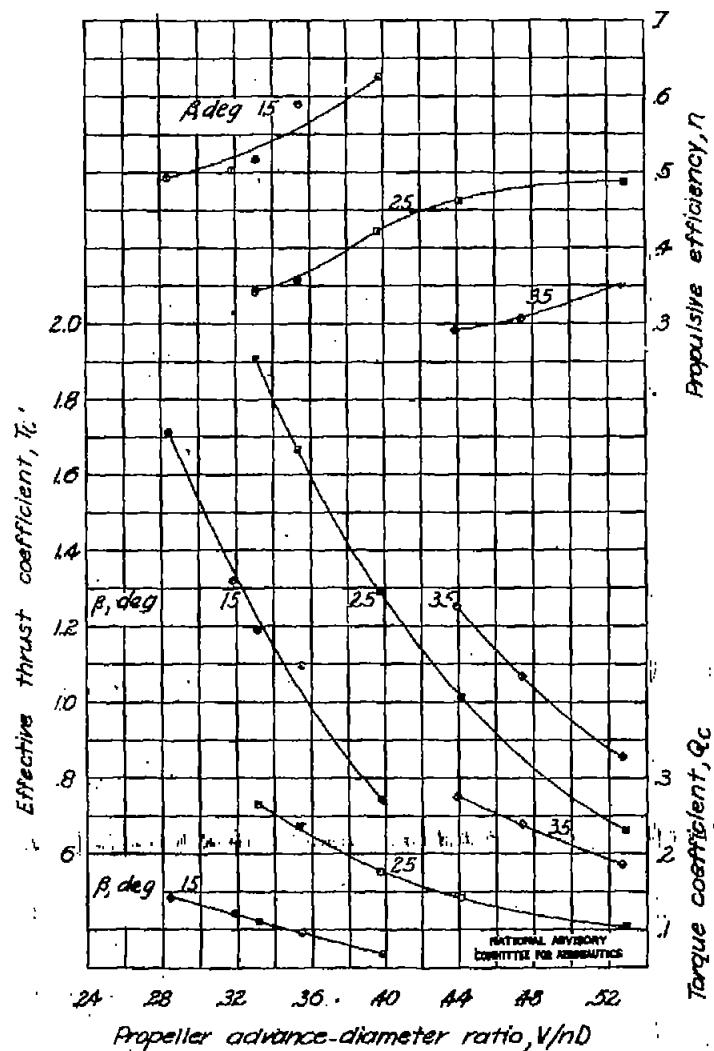
Figure 7 :- Propeller calibration of the single-engine low-wing fighter model. $\delta_f = 0°$; $a = 0°$; $D = 2.27$ ft; $q = 4.09$ lb/sq ft.
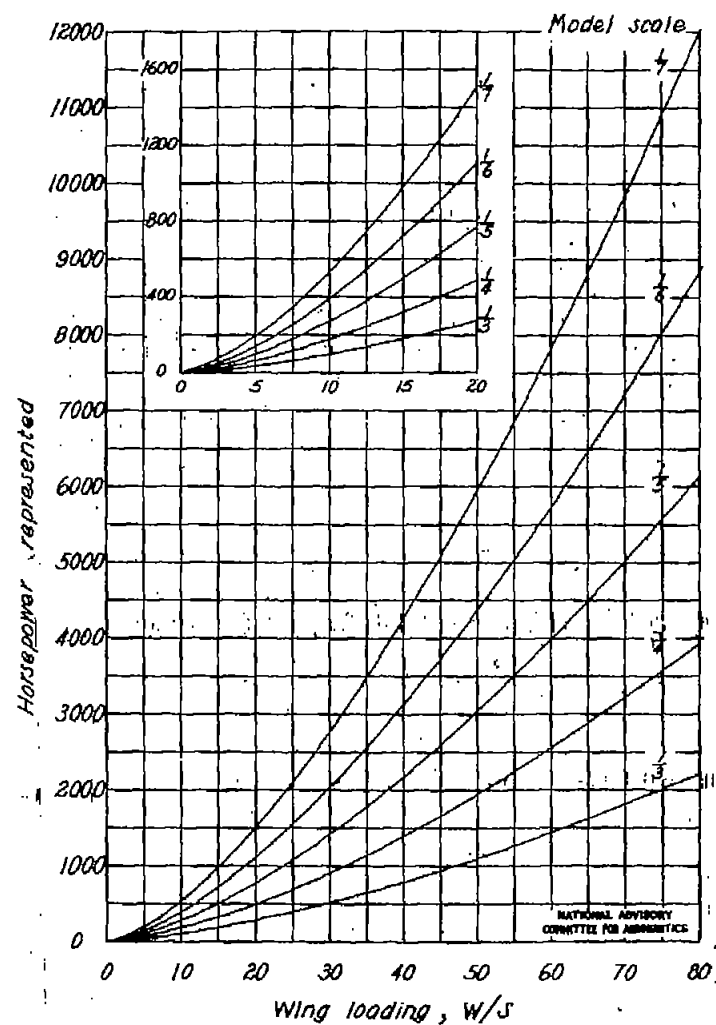
Figure 8 .- Horsepower represented for various wing loadings and model scales. $T_c = 1.25$; $C_L = 2.5$.
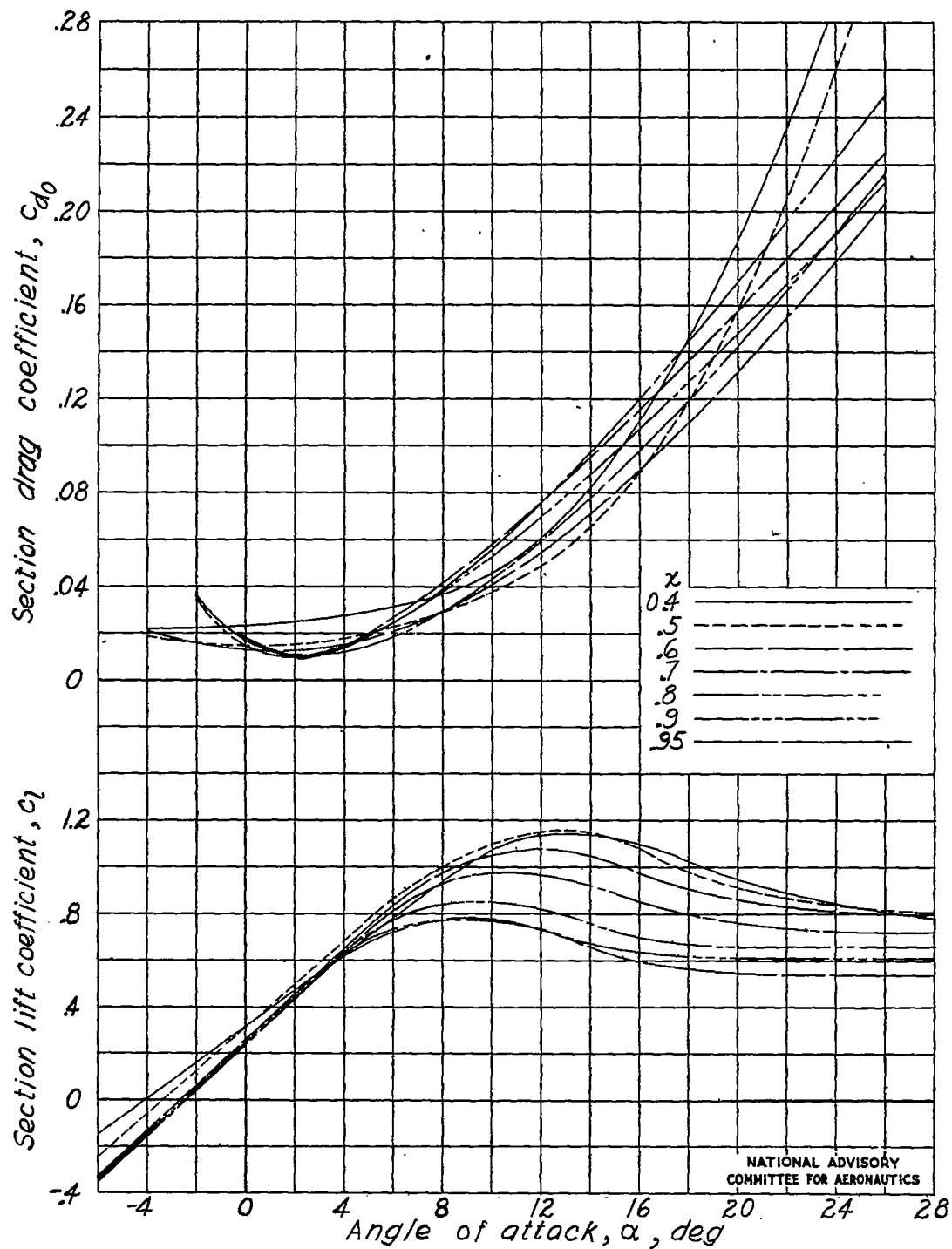
Figure 9 :-Blade section lift and drag curves for
the propeller used on the single-engine low-wing
fighter model. Estimated from references 8 to
10 ; average blade section Reynolds number,
350,000 (approx.).
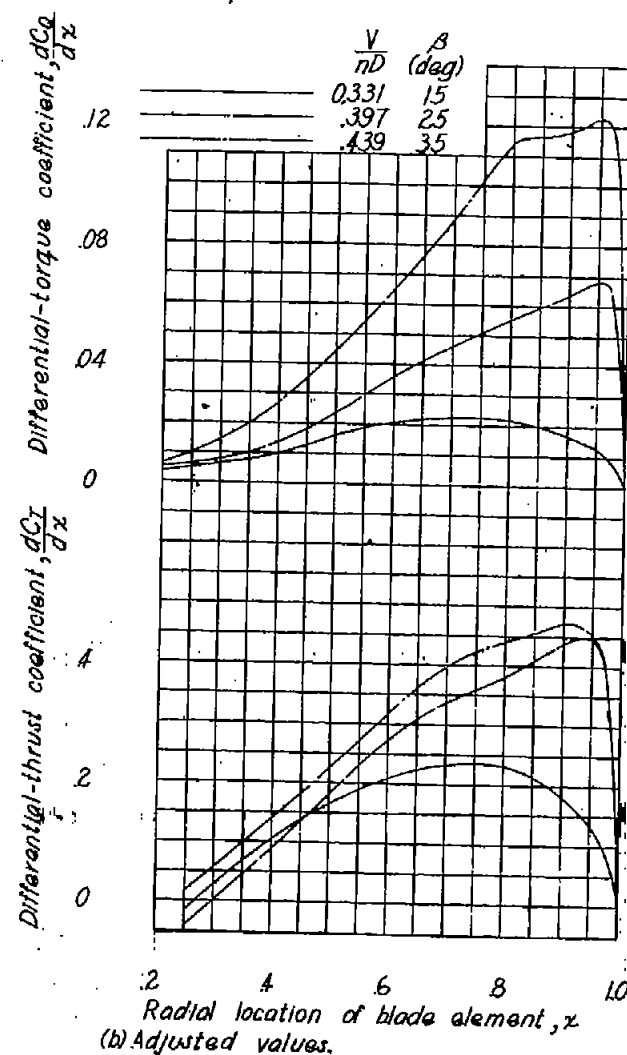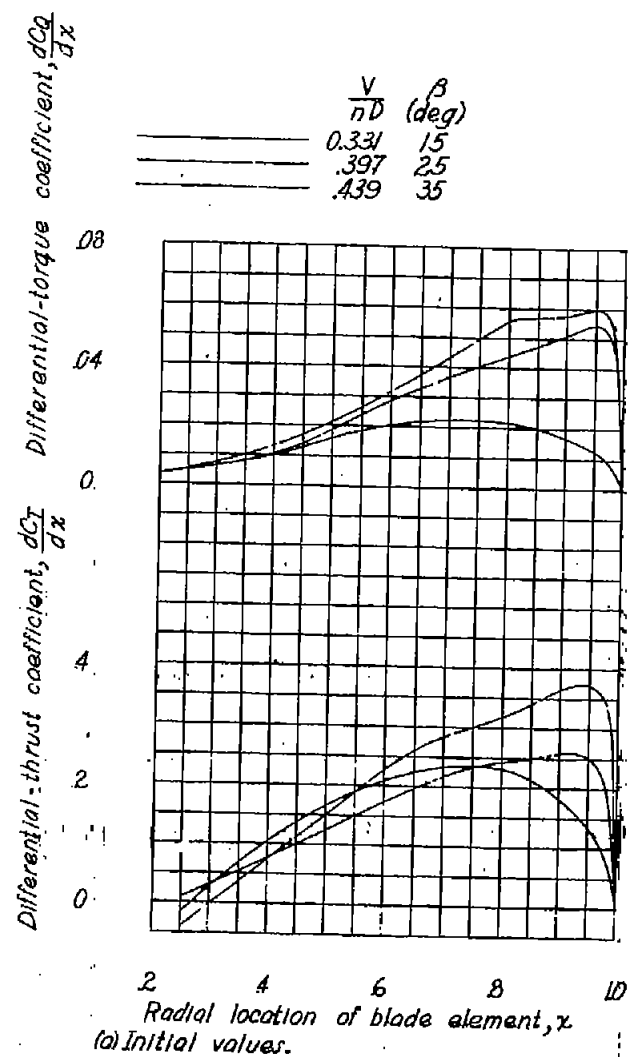
Figure 10.- Computed differential-thrust and torque-
distribution curves for the three-blade single-rotation
model propeller. $x = \frac{r}{R}$; r, station radius; R, tip radius.

(a) Initial values.

(b) Adjusted values.
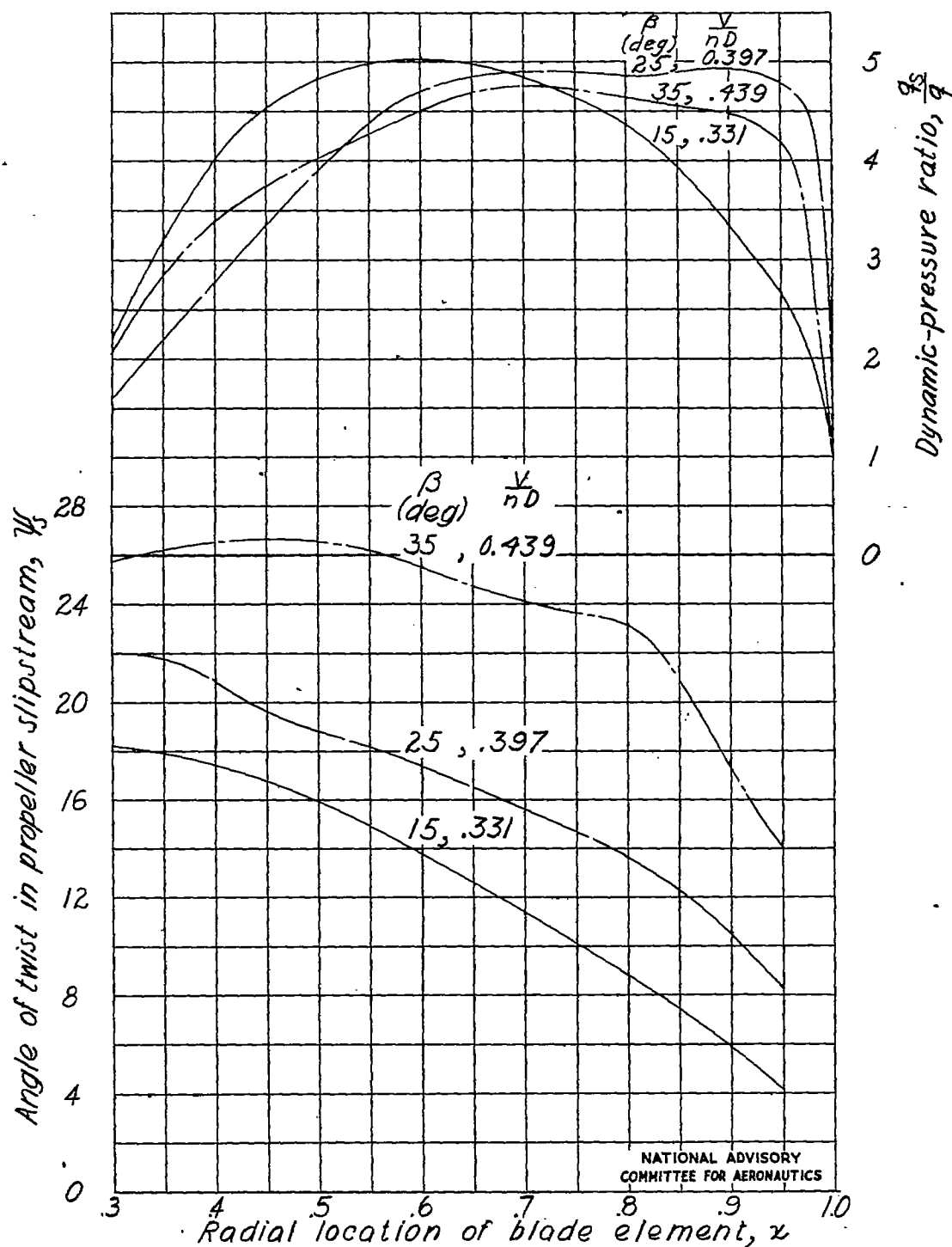
Figure 11.- Computed dynamic-pressure ratios and rotation distributions behind the propeller. $x = \frac{r}{R}$; R, radius; r, section radius.
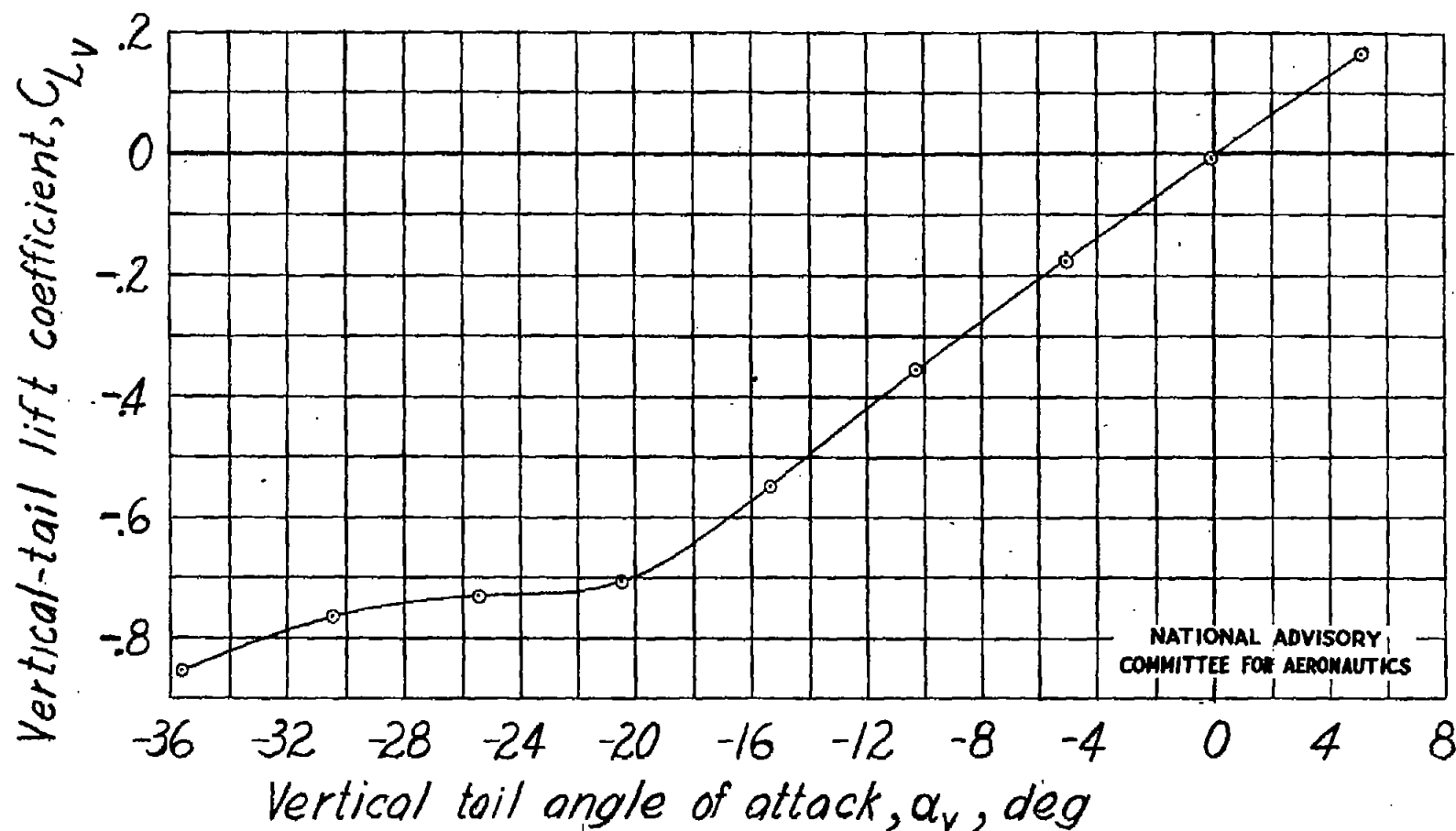
Figure 12.- Lift curve of the isolated vertical tail of the single-engine low-wing fighter model. $\delta_r = 0°$; $\delta_{r_T} = 0°$; $q = 15$ lb/sq ft.

Fig. 12

Figure 13.- Comparison of force and moment coefficients from tests and computations. $\psi = 0°$; $\alpha = 0°$ (approx).

Lateral-force coefficient C_Y

Rolling-moment coefficient C_l

Yawing-moment coefficient C_n

β
(deg)
• 15
□ 25
◆ 35

Pitching-moment coefficient C_m

Lift coefficient C_L

Longitudinal-force coefficient C_X

β
(deg)
• 15
□ 25
◇ 35

Angle of yaw, ψ, deg

Angle of yaw, ψ, deg

NATIONAL ADVISORY
COMMITTEE FOR AERONAUTICS

NATIONAL ADVISORY
COMMITTEE FOR AERONAUTICS
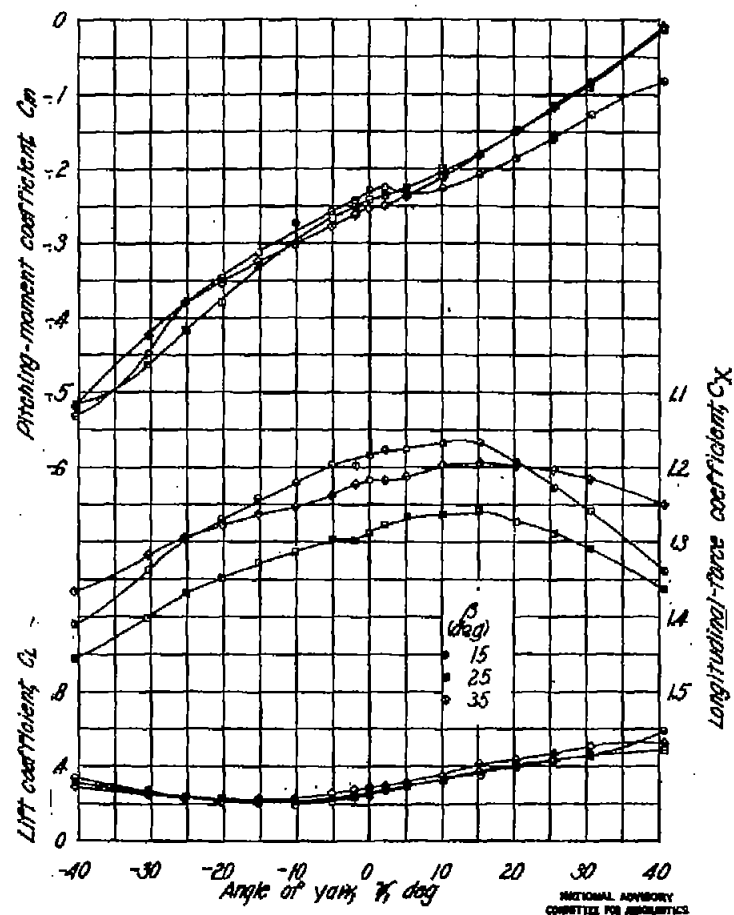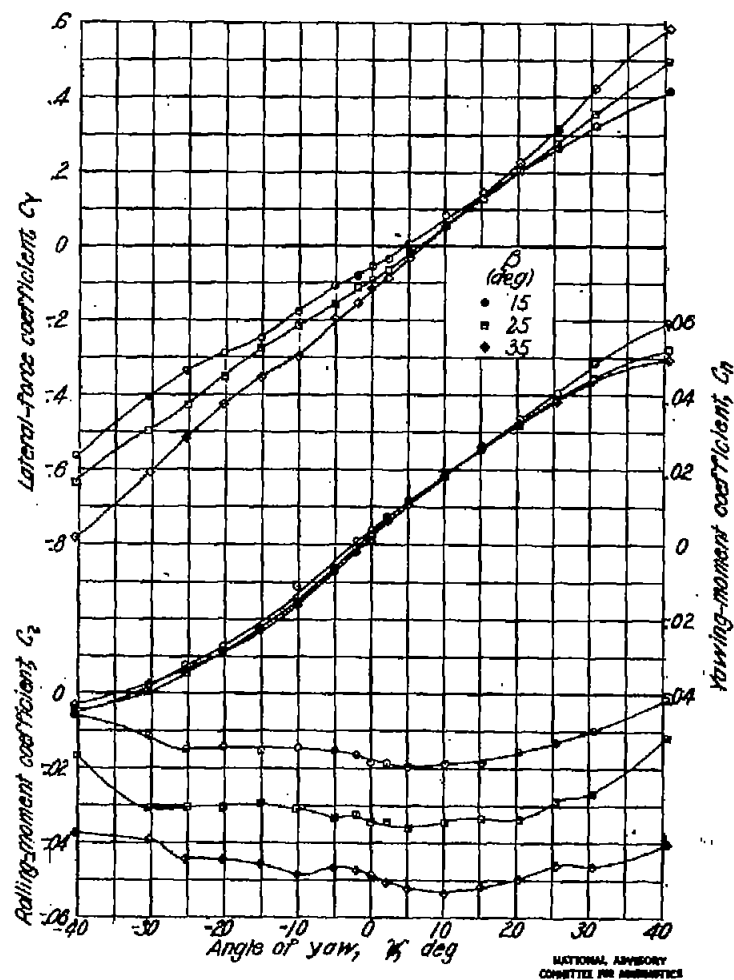
(a) Tail off.

Figure 14.-Effect of slipstream rotation on the
characteristics in yaw of the single-
engine low-wing fighter model. Short
tail; α = -0.2°; q = 4.09 lb/sq ft; T_c' = 1.25 (approx).

(b) Tail on, $\delta_r = 0°$, $\delta_{rr} = 0°$.

Figure 14. Continued.

(c) Tail on, rudder free, $\delta_{r_f} = 0°$.

Figure 14-Continued.

β
(deg)
25
35
15
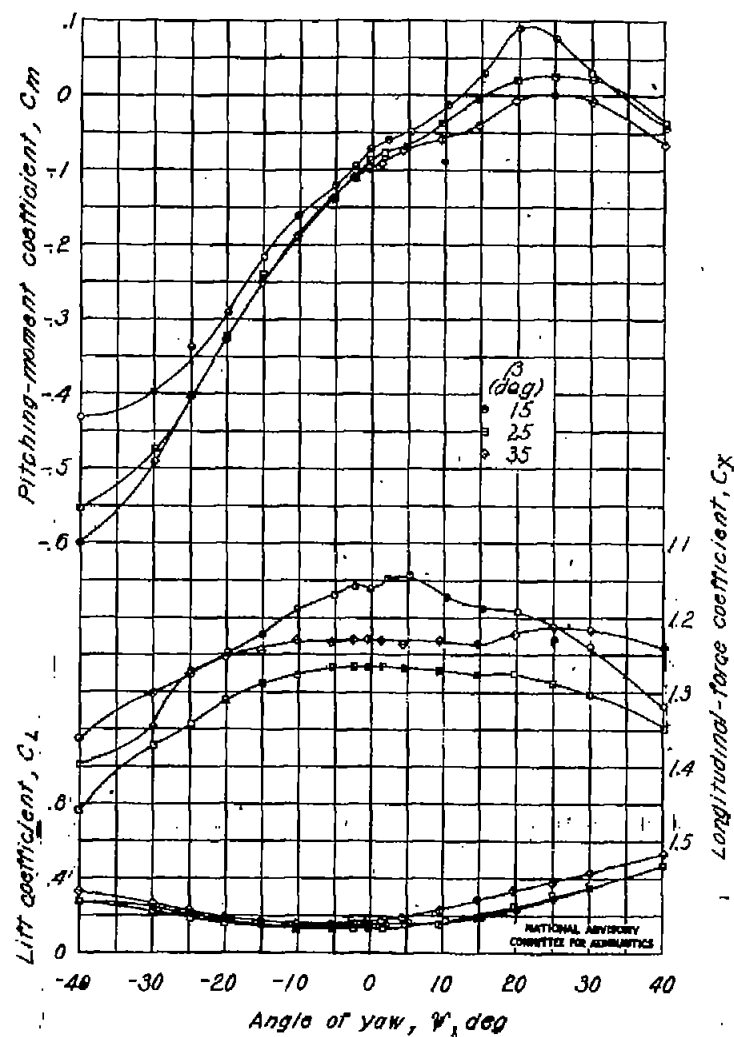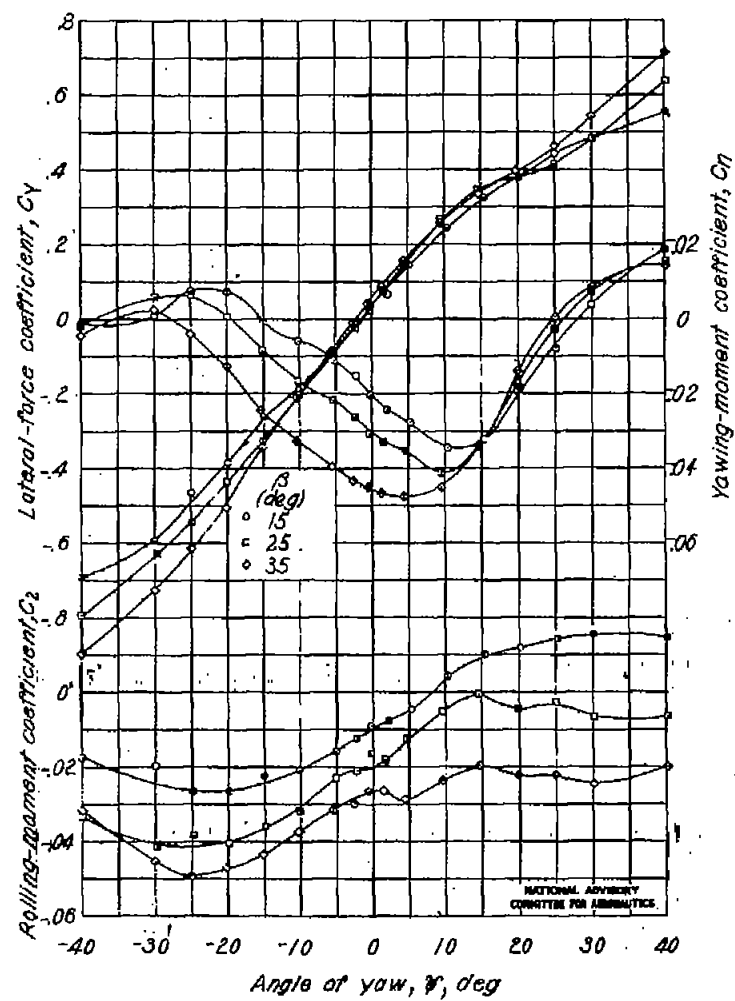
(c) Concluded.
Figure 14.-Concluded.
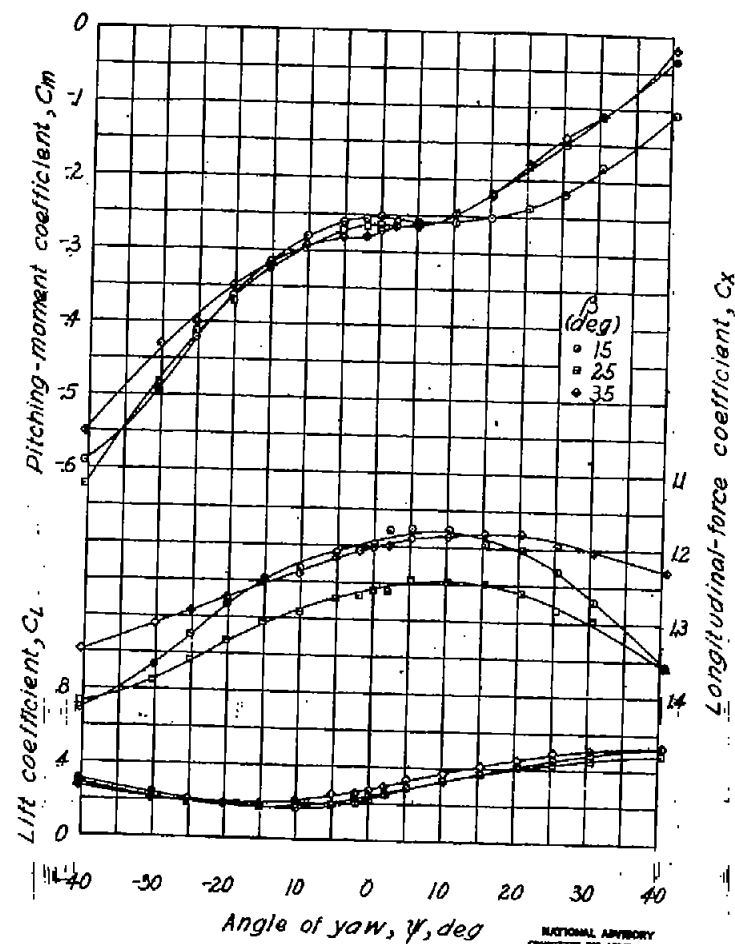
NATIONAL ADVISORY
COMMITTEE FOR AERONAUTICS

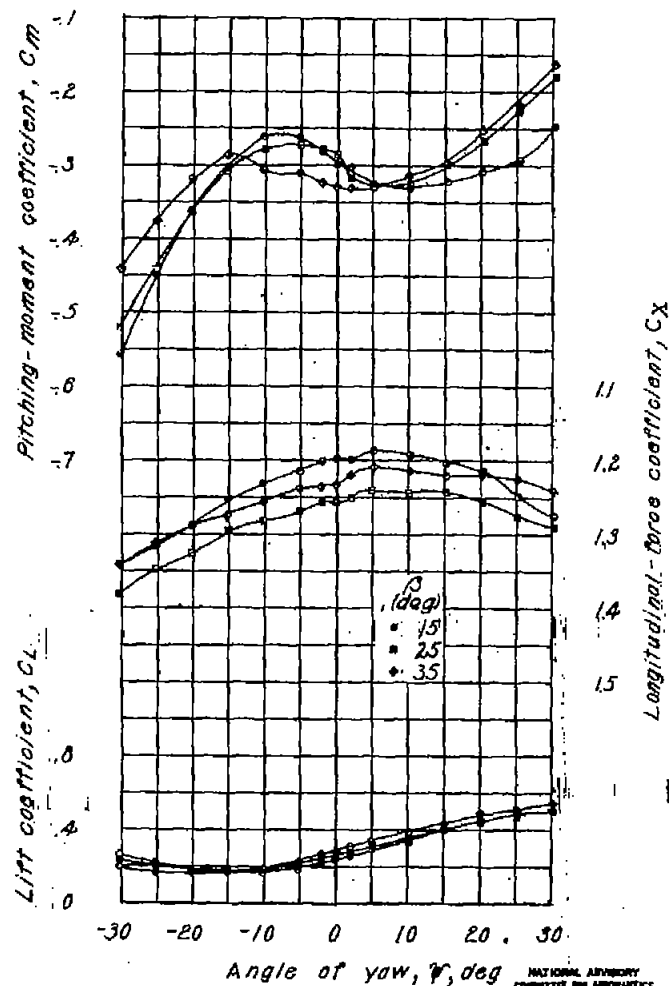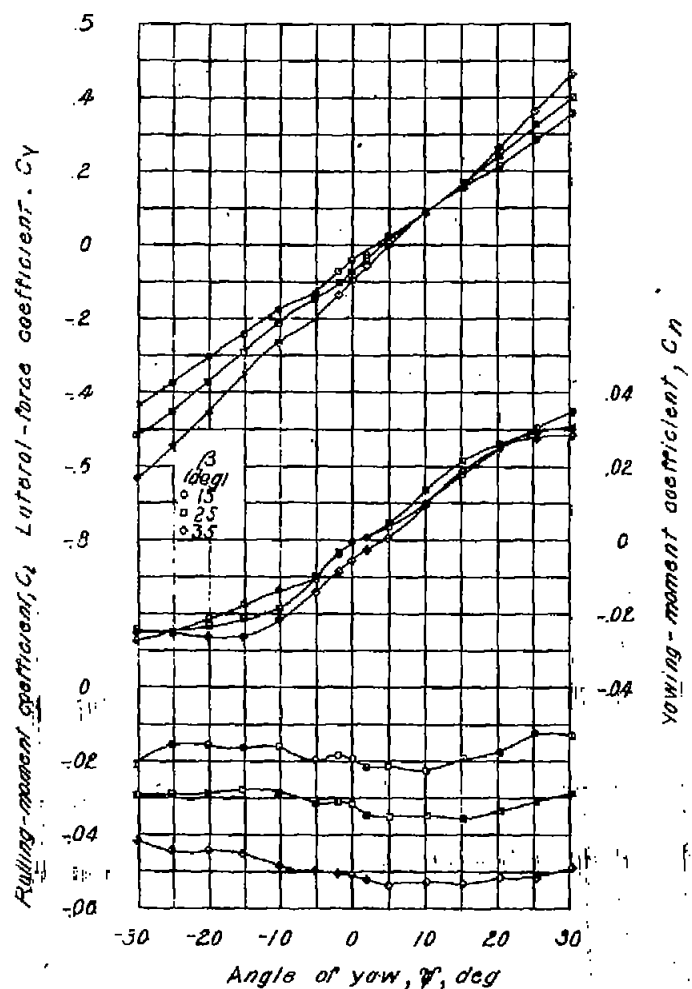Figure 15.- Effect of slipstream rotation on the
characteristics in yaw of the single-engine
low-wing fighter model. Normal tail;
$\alpha = -0.2°$; $q = 4.09 \ lb / sq \ ft$; $T_c' = 1.25 \ (approx)$.

(a) Tail off.
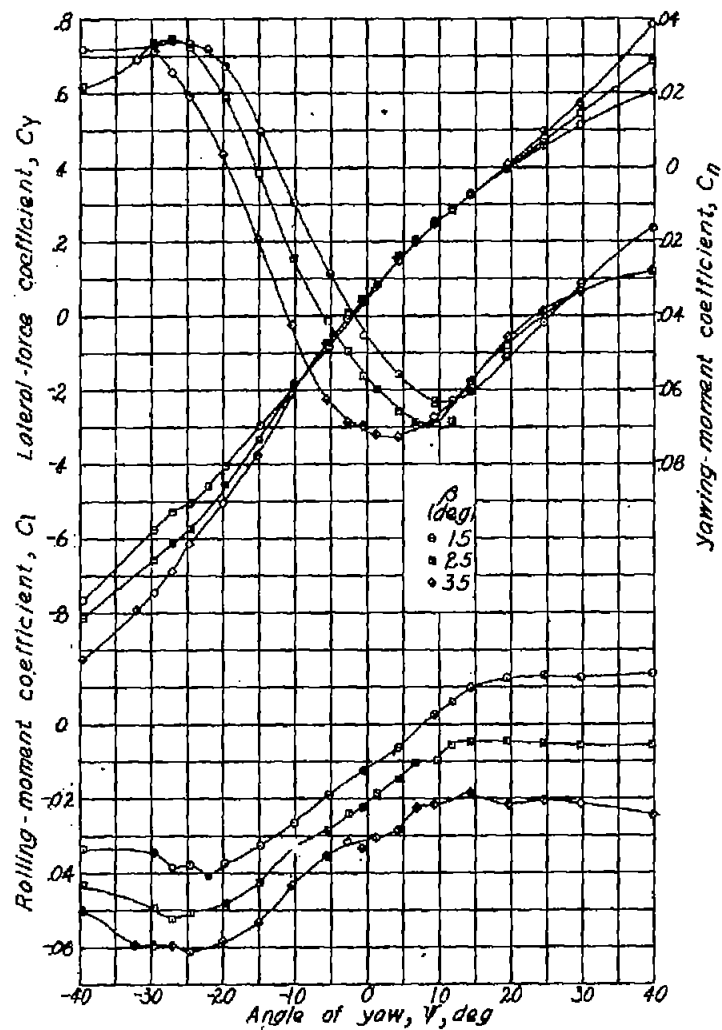
(b) Tail on, $\delta_r = 0°$, $\delta_{rr} = 0°$.

Figure 15.-Continued.
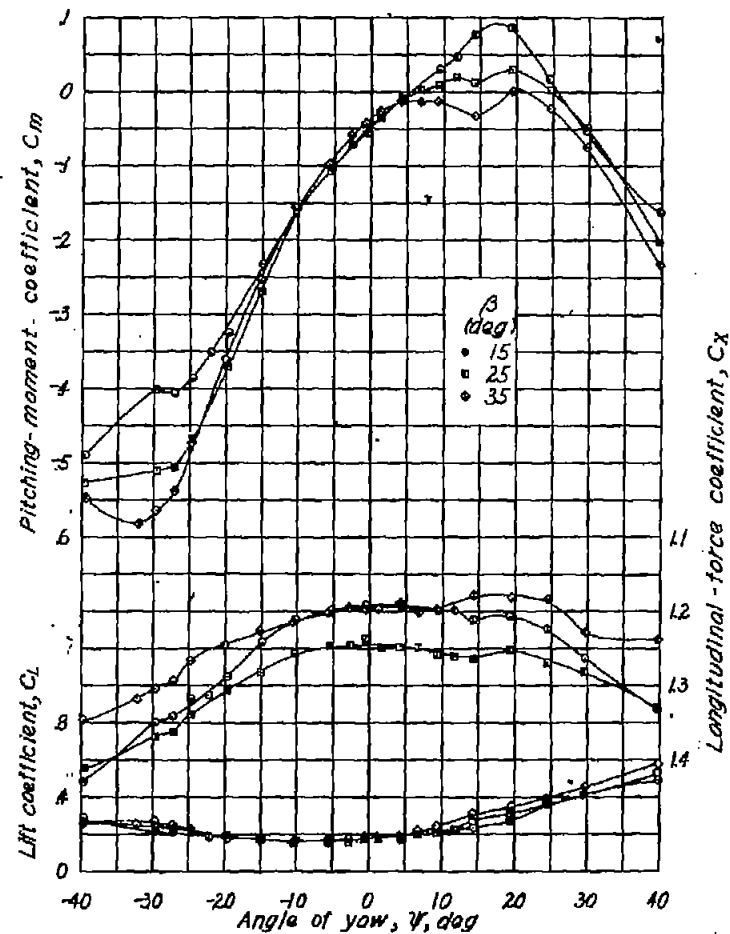
NATIONAL ADVISORY
COMMITTEE FOR AERONAUTICS
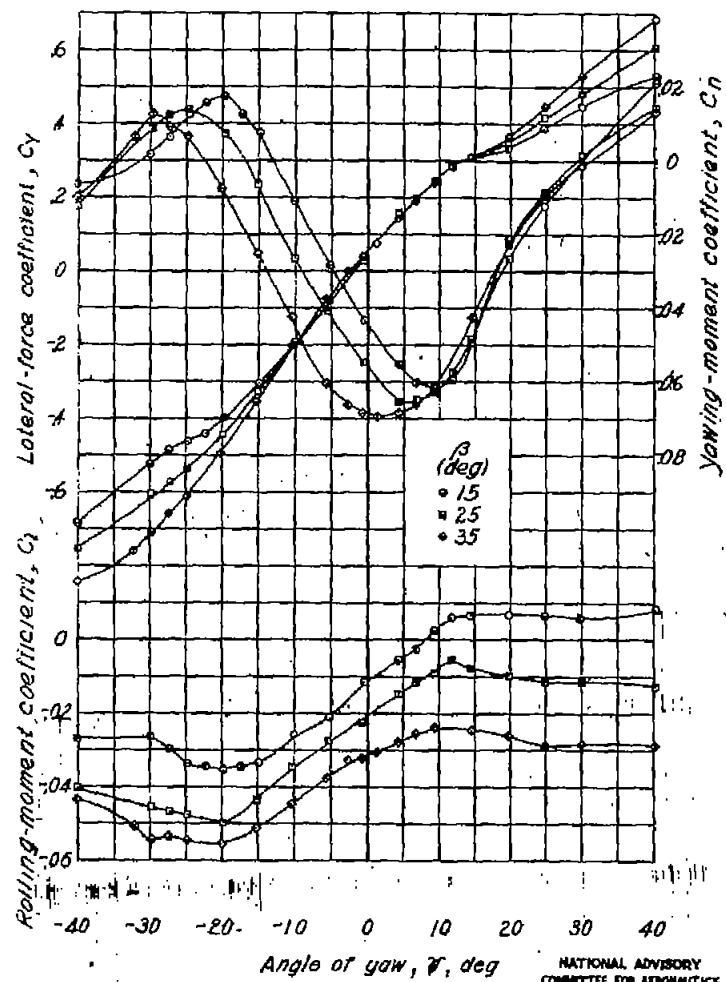
(c) Tail on, rudder free, $\delta_r = 0°$.

Figure 15-Continued

(c) Concluded.
Figure 15. Continued.
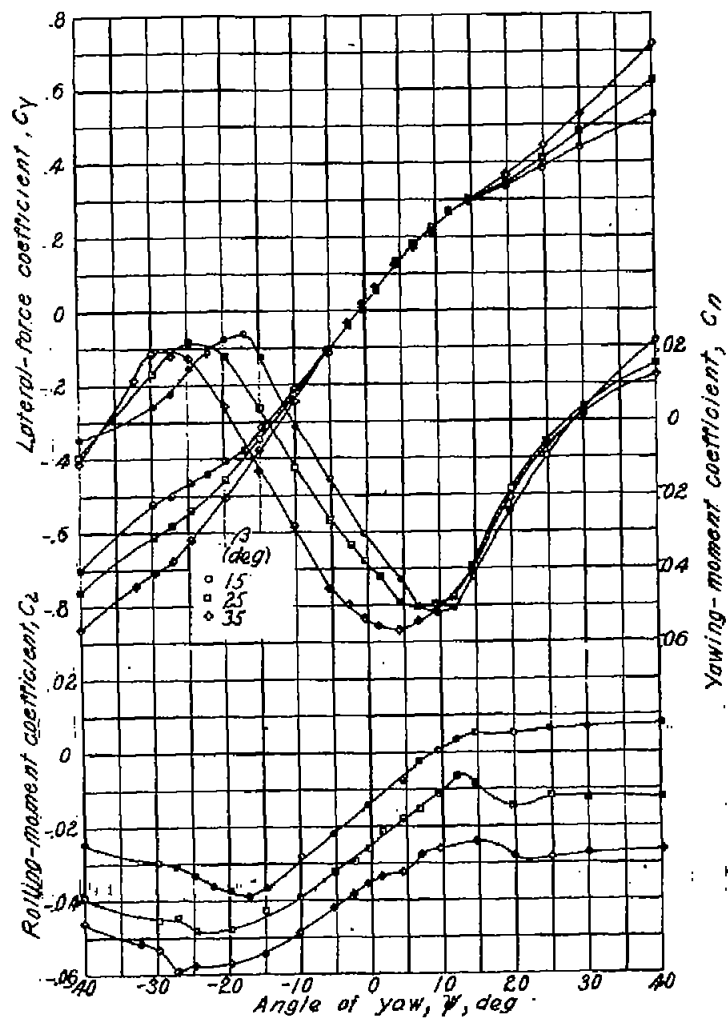
(d) Tail on, rudder free, $\delta_r = 20°$

Figure 15.- Continued.

Angle of yaw, ψ, deg
(d) Concluded.
Figure 15.- Concluded.
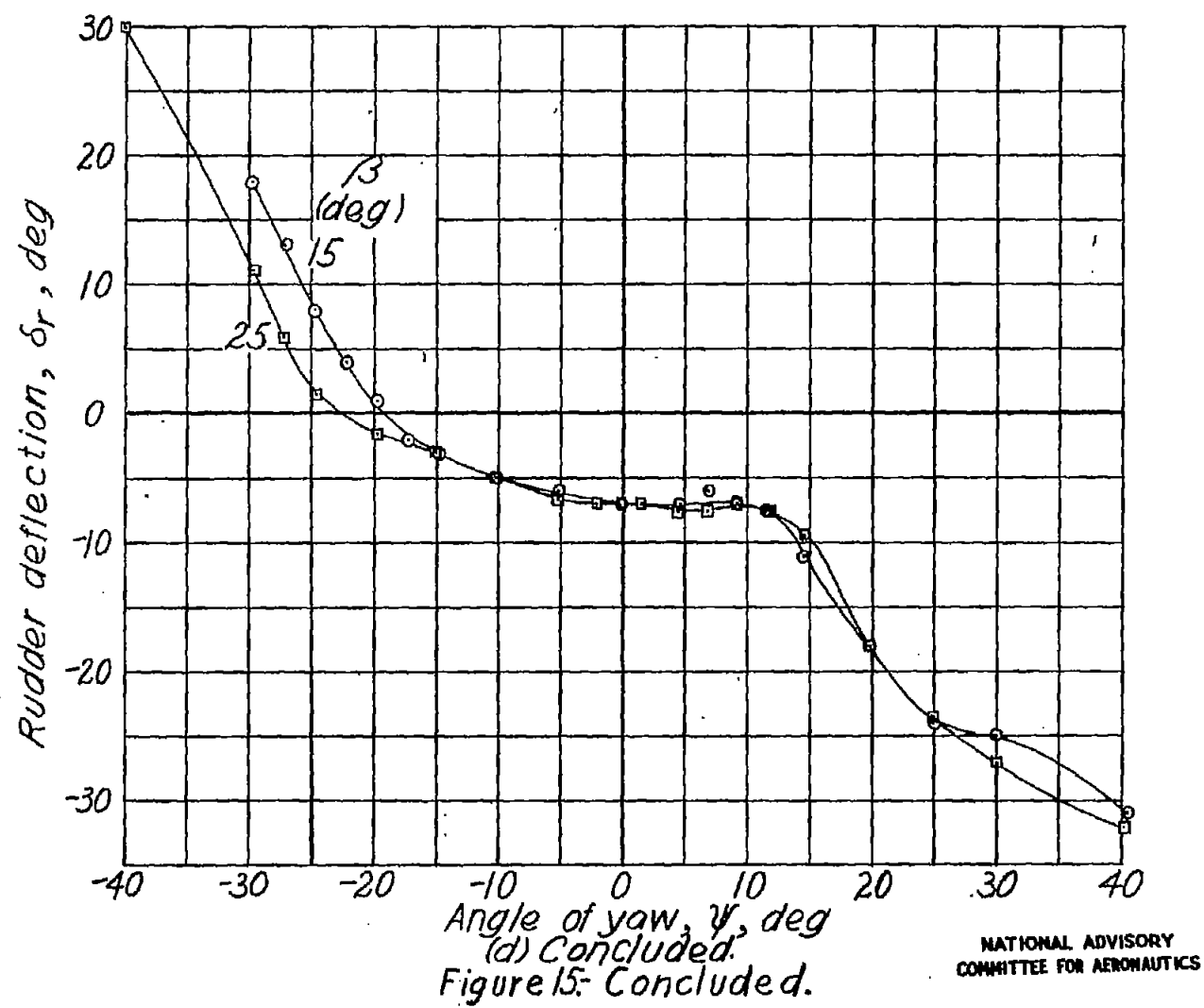
(a) Tail off.

Figure 16.- Effect of slipstream rotation on the characteristics in yaw of the single-engine low-wing fighter model. Long tail; α=-0.2; q=40.9 lb/sq ft; T'c≈1.25. (approx).
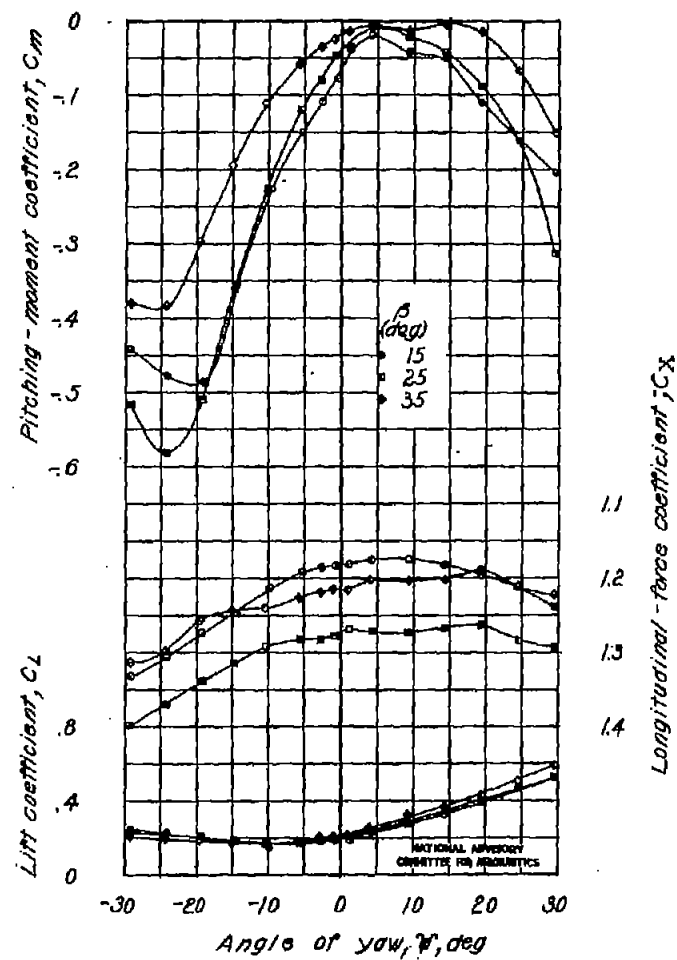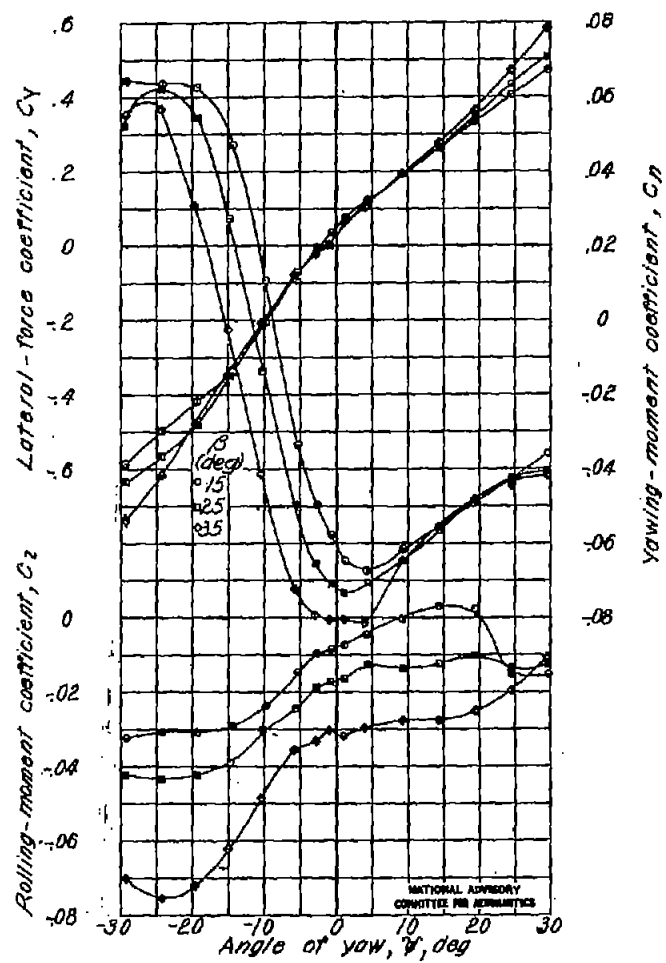
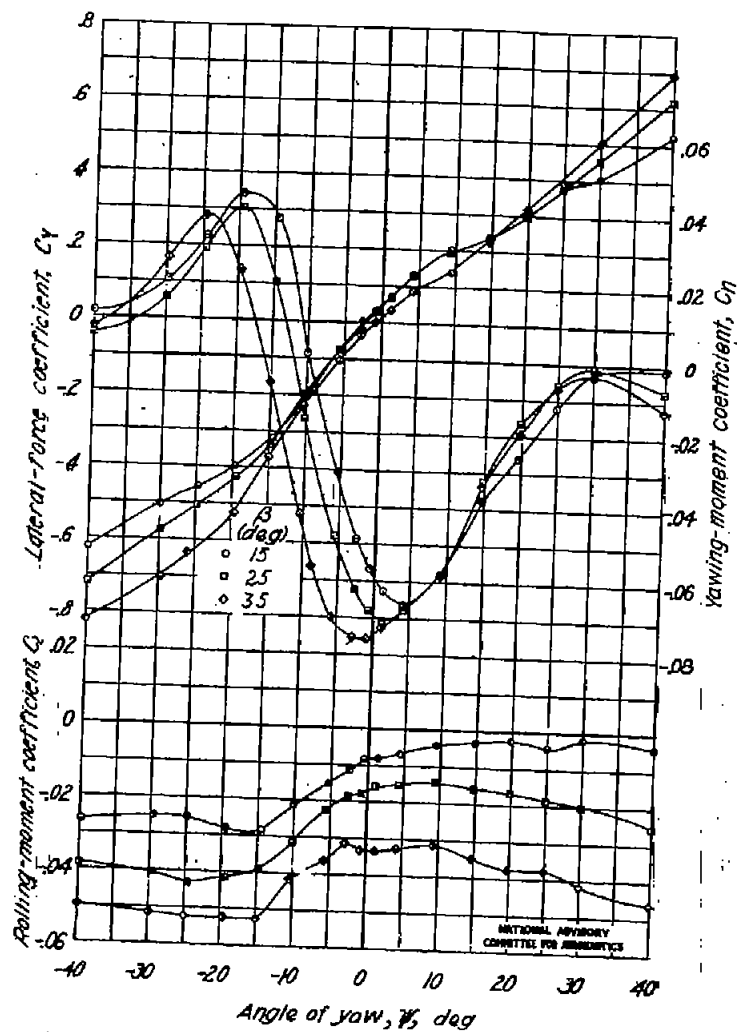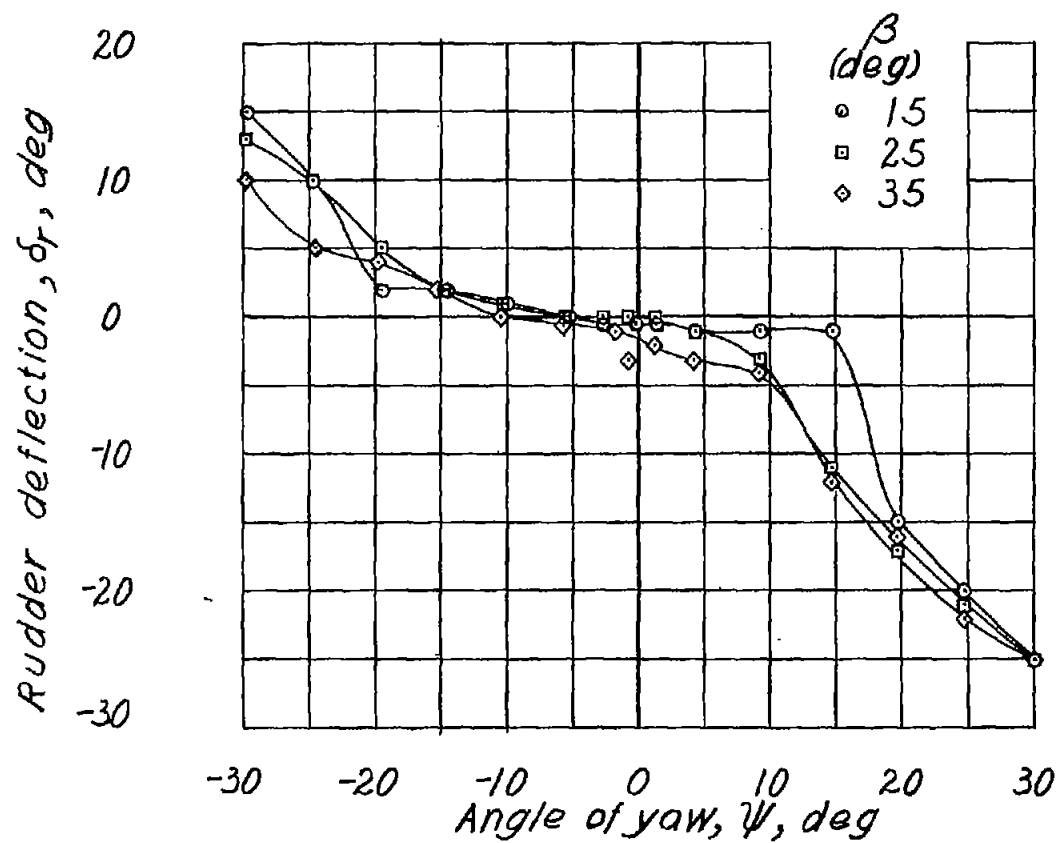(b) Tail on, $\delta_r = 0°$, $\delta_{rr} = 0°$;
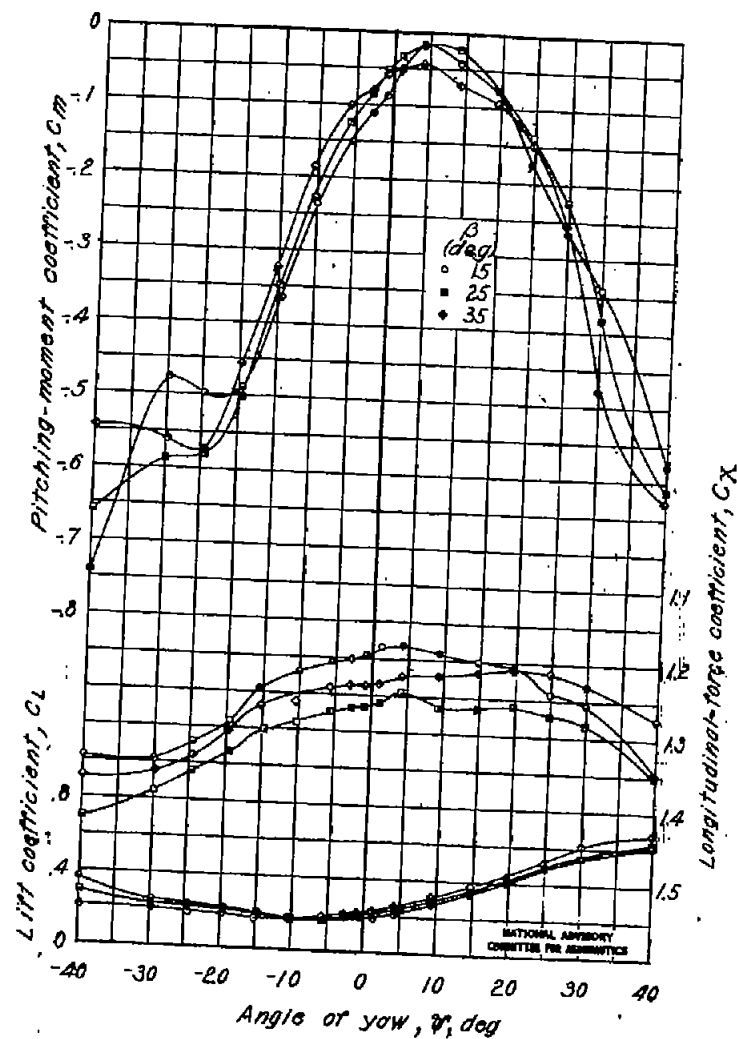
Figure16.-Continued.

(c) Tail on, rudder free, $\delta_{rr} = 0°$.

Figure 16.-Continued

(c) Concluded.

Figure 16.-Concluded.

NATIONAL ADVISORY
COMMITTEE FOR AERONAUTICS